INTEGRATED OPTIC WAVEGUIDES

WAVEGUIDES, PLANAR

WAVEGUIDES, OPTICAL

INTRODUCTION

Integrated optics is concerned with the integration of various kinds of miniaturized optical devices onto a single substrate to form optical integrated circuits, and can be viewed as the optical counterpart of integrated electronics. By integration, a complex optical system, which could occupy a desk-sized optical bench if assembled with bulk optical components, may be implemented on a small optical chip with the size of a coin. A packaged optical chip may incorporate optical fiber pigtails at its input and output ports, so that it can be readily connected to an optical fiber network. The merits of integration are obvious; it allows the realization of compact, robust, and stable devices, and could lead to cost-effective products.

Since the concept of integrated optics was introduced in 1969 (1, 2), it has evolved into a well-respected discipline. Integrated optics has widened the scope of application of optics considerably, and contributed significantly to the advancement of several important applications, including optical communication, optical sensing, and optical signal processing. For the last twenty years or so, considerable efforts have been devoted to the integration of both optical components and electronic components on a single substrate to form monolithic integrated circuits. This technology goes beyond integrated optics and is commonly known as integrated optoelectronics. Detailed accounts of the developments in integrated optics at different stages can be found, for example, in references 1–10.

Optical devices can be broadly divided into two types: passive devices, such as directional couplers, beam splitters, filters, wavelength multiplexers, etc., which do not require external electric sources; and active devices, such as lasers, modulators, switches, etc., which require external electric sources. In an optical integrated circuit, the problem of connecting various components or devices is solved by the use of optical waveguides. An optical waveguide is a long thin structure which, in general, consists of a layer of high-index dielectric medium surrounded by one or more low-index media. Such a structure, when properly designed, is capable of trapping light in the high-index layer and guiding it along the medium. Because of this property, light can be directed precisely from one place to the other via an optical waveguide. A well-known example of an optical waveguide is the optical fiber, which has a circular core surrounded by a cladding with a slightly lower index. Waveguides used in integrated optics, however, are exclusively of thin-film type, as they must be fabricated on planar substrates. Figure 1 shows some common integrated optical waveguide geometries, where the shaded areas highlight the high-index layers. Because the optical wavelength is of the order of 1 μm, the thickness of the high-index guiding layer in an optical waveguide is typically of the order of $1 - 10$ μm. The length of a typical waveguide varies from several hundred micro-meters to a few centi-meters, which is long, compared with the wavelength.

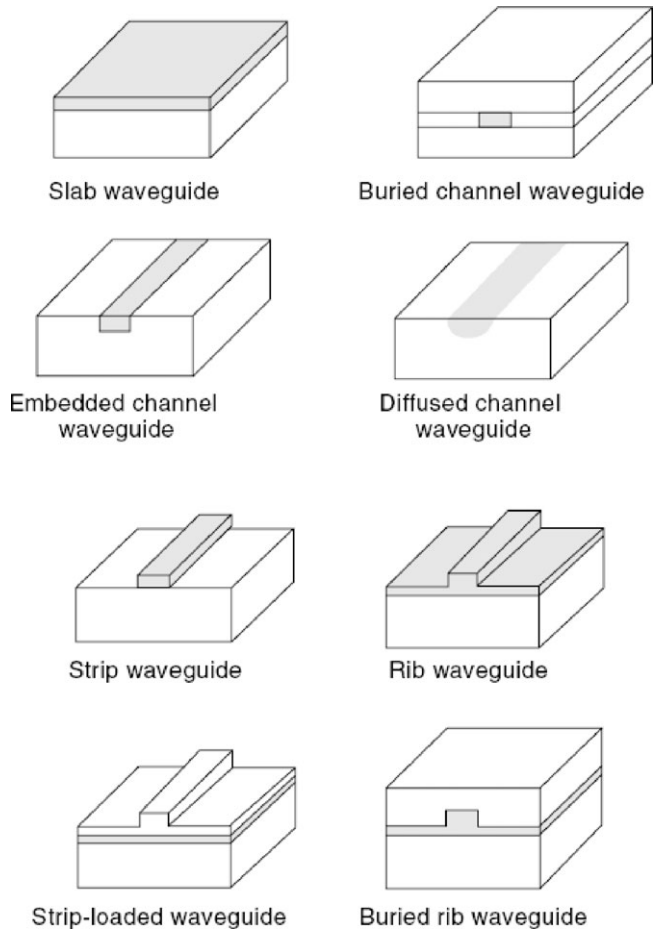

Figure 1. Some common integrated optical waveguides.

Apart from providing the necessary connections, optical waveguides also serve as the building blocks of many optical devices. To prevent light from diffracting away when coupled into, or out of, an optical device, it should preferably be contained within a waveguide, and remain guided everywhere in the circuit. This requirement calls for the design and fabrication of a whole range of novel waveguide-based optical devices. Such devices differ markedly from their counterparts based on bulk optics, not only in the physical appearance, but also in the operational principles and performance. Integrated optical devices have varying requirements on materials and waveguide geometries, so that many different waveguide structures (see Fig. 1) have been developed for various applications. Waveguide geometry can also be dictated by the fabrication technique, which is often developed specifically for certain materials. For example, buried square-core waveguides with silica glasses are particularly suitable for forming passive devices that are connected directly to optical fibers, owing to the fact that the optical properties of these waveguides

J. Webster (ed.), *Wiley Encyclopedia of Electrical and Electronics Engineering*. Copyright © 2007 John Wiley & Sons, Inc.

match closely with those of optical fibers. On the other hand, strip-loaded and rib waveguides are more compatible with active semiconductor devices and lasers based on gallium arsenide or indium phosphide. Graded-index channel waveguides are the products of the ion-diffusion process on glasses and electro-optic crystals (such as lithium niobate and lithium tantalate). The embedded channel geometry makes easier the deposition of electrodes close to the waveguide and is the preferred geometry for the implementation of electro-optic interactions. In general, it is difficult to integrate different kinds of devices on the same substrate material. Over the years, however, significant progress has been made in achieving monolithic integration based on semiconductor materials (4,6,8,10).

To understand the operation of waveguide-based devices, we must first understand how light propagates in an optical waveguide. The most fundamental property of an optical waveguide is the presence of guided modes (or guided waves). A guided mode is a light wave that propagates along the waveguide at a constant phase velocity and has a well-defined optical field distribution. Provided that the waveguide is uniform in the direction of light propagation, the field distribution of a guided mode does not change with the distance that the light travels. A waveguide that allows more than one guided mode to propagate is referred to as a multimode waveguide, in contrast with a single-mode waveguide that supports only one guided mode. The central problem in analyzing an optical waveguide is the calculation of the phase velocities and the field patterns for the modes of the waveguide. The importance of knowing the modes lies in the fact that a superposition of the mode fields can represent an arbitrarily complicated field distribution. This has direct application in solving, for example, waveguide excitation and jointing problems. The principle of superposition also forms the basis of the powerful coupled-mode theory, which can be applied to a wide variety of complicated situations including non-uniform structures, yet requires only the solutions for the modes of uniform waveguides. We may say that the theory of optical waveguides is largely built upon the concept of modes. Detailed treatments of various theoretical aspects of optical waveguides are given in references 11–17.

PLANAR WAVEGUIDES

We begin with the simplest waveguide, the planar waveguide, which is capable of confining light in one dimension. There are two types of planar waveguide: the step-index slab waveguide and the graded-index waveguide, which differ from each other in the form of the refractive-index distribution (or profile).

Three-Layer Step-Index Slab Waveguides

Figure 2 shows the geometry and the refractive-index profile of a three-layer step-index slab waveguide, which consists of a thin film (guiding layer) of refractive index n_1 and thickness $2t$ sandwiched between a substrate and a cover material with lower refractive indices n_2 and n_3 ($n_1 > n_2 \geq n_3$). Light is confined in the x direction and propagates in the z direction. We first use a zig-zag wave model

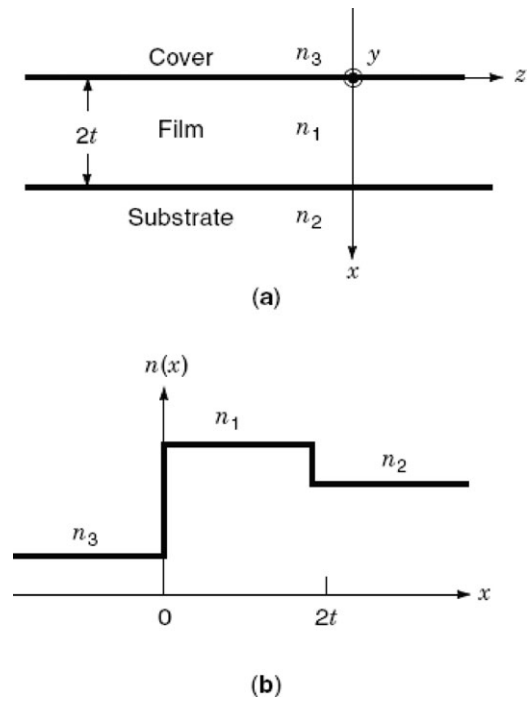

Figure 2. (a) Geometry and (b) refractive-index profile of a step-index slab waveguide formed by sandwiching a high-index layer (film) between two low-index layers (cover and substrate).

(2) to develop an intuitive picture of wave propagation in the waveguide and then outline the more rigorous treatment based on the electromagnetic theory.

Zig-zag wave model. Consider a plane wave which is incident upon an interface between two different media. When the angle of incidence measured between the direction of incidence and the normal to the interface is larger than the critical angle, the light wave undergoes total internal reflection. The critical angles at the cover-film and substrate-film interfaces are given, respectively, by

$$\theta_c = \sin^{-1}(n_3/n_1) \tag{1}$$

and

$$\theta_s = \sin^{-1}(n_2/n_1). \tag{2}$$

Because $n_2 \geq n_3$, it follows that $\theta_s \geq \theta_c$. A guided wave can be understood as a light wave that undergoes total internal reflections at both cover-film and substrate-film interfaces and propagates along the film in a zig-zag manner, as shown in Fig. 3(a), where θ denotes the angle of incidence at the interfaces. The condition $\pi/2 > \theta > \theta_s$ must therefore be satisfied for a guided wave to exist. In the case that $\theta_s > \theta > \theta_c$, light escapes to the substrate, whereas in the case that $\theta_c > \theta$, light escapes to both the cover and the substrate. The light waves in these two cases are called radiation modes, which are not confined in the film. The condition $\theta = \theta_s$ is called the cut-off condition.

Consider a monochromatic wave with complex time and z dependences in the form $exp[j(\omega\tau - \beta z)]$, where $j \equiv \sqrt{-1}$, τ is time, ω is the radian optical frequency, and β is the propagation constant or phase constant. The phase velocity

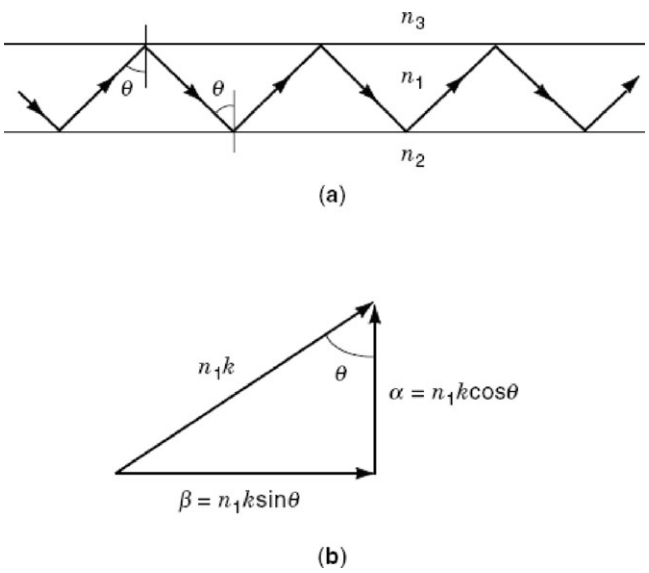

Figure 3. (a) A guided wave in a step-index slab waveguide can be modeled by a zig-zag wave bouncing up and down in the film under total internal reflections. (b) The z component of the wave vector of the zig-zag wave gives the propagation constant β of the guided wave, while the x component gives the phase constant α in the x direction.

of the wave is given by $v_p = \omega/\beta$. As shown in Fig. 3(b), the propagation constant is simply the z component of the wave vector, i.e., $\beta = n_1 k \sin\theta$, where $k = 2\pi/\lambda$ is the free-space wavenumber (or free-space propagation constant of the plane wave) and λ is the free-space wavelength. From the range of θ for a guided wave, it is easy to show that

$$n_1 > \frac{\beta}{k} > n_2. \tag{3}$$

The dimensionless parameter β/k can be understood as the effective refractive index seen by the wave, and is often referred to as the effective index or mode index. When the mode is at cut-off, $\beta/k = n_2$.

Not every value of β/k that satisfies Eq. (3) represents a physical guided wave. Suppose we travel in the z direction along with the wave at its phase velocity. We should always see the same phase of the guided wave, i.e., the same field distribution in the transverse direction. The guided wave must therefore have a field distribution in the x direction that is invariant in the z direction. However, according to the zig-zag wave model shown in Fig. 3(a), what we see also are plane waves that bounce up and down within the film. To obtain a z-invariant field distribution in the x direction, such plane waves must form a standing wave in the x direction. To form a standing wave, the phase acquired by the plane waves after traveling a round trip in the x direction must be equal to an integral number of 2π:

$$4t\alpha - 2\Phi_2 - 2\Phi_3 = 2m\pi, \quad m = 0, 1, 2, \ldots, \tag{4}$$

where $4t\alpha$ represents the phase acquired in the film with $\alpha = n_1 k \cos\theta$ being the phase constant in the x direction, as shown in Fig. 3(b), and $-2\Phi_2$ and $-2\Phi_3$ represent the phase shifts acquired by the wave under total internal reflections at the substrate and cover interfaces, respectively. Equation (4) is known as the transverse resonance condition. It is obvious that Eq. (4) admits only discrete incidence angles.

The guided waves in a slab waveguide can have two orthogonal polarizations. The wave that is linearly polarized in the y direction is called the TE (transverse electric) mode, because it has a single electric-field component in the y (transverse) direction. The wave that is linearly polarized in the direction that is perpendicular to both the y direction and the wave vector is called the TM (transverse magnetic) mode, because it has a single magnetic-field component in the y direction. It should be noted that the TE mode has magnetic-field components in both the x and z directions, while the TM mode has electric-field components in both the x and z directions. It is known that the phase shifts $-2\Phi_2$ and $-2\Phi_3$ depend on the polarization of the wave (see, for example, chapter 2 of reference 4). By using the mode index instead of the angle of incidence as the parameter, the transverse resonance condition Eq. (4) can be written as

$$2tk[n_1^2 - (\beta/k)^2]^{1/2} = m\pi + \Phi_2 + \Phi_3, \quad m = 0, 1, 2, \ldots, \tag{5}$$

with

$$\Phi_i = \tan^{-1}\{r_i[\frac{(\beta/k)^2 - n_i^2}{n_1^2 - (\beta/k)^2}]^{1/2}\}, \quad i = 2 \text{ or } 3, \tag{6}$$

where the factor r_i distinguishes between the TE and TM modes, with $r_i = 1$ for the TE mode and $r_i = (n_1/n_i)^2$ for the TM mode. For a given free-space wavenumber k (or wavelength λ), the effective indices β/k for all the guided modes can be found from Eq. (5) by a root-searching technique. The integer m in Eq. (5) is called the mode order and the modes are labeled as TE_m and TM_m modes.

In many practical applications, the refractive index of the thin film is only slightly larger than that of the substrate (the difference is of the order of one percent), i.e., $n_1^2 - n_2^2 \ll n_1^2 - n_3^2$. The phase shifts Φ_2 and Φ_3 ($\Phi_3 \cong \pi/2$) then become insensitive to the polarization of the wave and the effective indices of the TE and TM modes of the same order are nearly equal. In that case, the angle θ shown in Fig. 3(a) is close to $\pi/2$ and, as a result, the TM mode is approximately linearly polarized in the x direction with a negligible electric-field component in the z direction.

Putting $\beta/k = n_2$ into Eq. (5) results in an expression for the cut-off wavelength λ_c:

$$\lambda_c = \frac{4\pi t(n_1^2 - n_2^2)^{1/2}}{m\pi + \tan^{-1}(r_3\sqrt{a})}, \tag{7}$$

where

$$a = \frac{n_2^2 - n_3^2}{n_1^2 - n_2^2} \tag{8}$$

is a factor that measures the degree of asymmetry of the waveguide structure (with $a = 0$ for the symmetric case $n_2 = n_3$). As an example, with $n_1 = 1.55$, $n_2 = 1.50$, $n_3 = 1.0$ (air), and a film thickness of $2t = 1$ μm, the cutoff wavelengths for the TE_0, TM_0, TE_1, TM_1 modes are 1.987 μm, 1.720 μm, 0.561 μm, and 0.537 μm, respectively. If the operating wavelength is longer than 1.987 μm, the waveguide does not support any guided mode. If the wavelength lies between 1.720 μm and 1.987 μm, only the TE_0 mode

is supported and a single-mode waveguide results. As the wavelength becomes shorter and shorter, more and more modes are allowed to propagate.

The number of guided modes supported by the waveguide can be determined from m_c, the value of m evaluated at $\beta/k = n_2$:

$$m_c = \frac{4t}{\lambda}(n_1^2 - n_2^2)^{1/2} - \frac{1}{\pi}\tan^{-1}(r_3\sqrt{a}). \tag{9}$$

The next integer larger than m_c gives the number of modes. With the same refractive indices used in the previous example, at a wavelength of 1.3 μm, a film thickness of 1 μm gives $m_c = 0.21$ and for the TE and TM modes, respectively. The waveguide therefore supports only the TE_0 and TM_0 modes. If the film thickness is increased to 10 μm, we find $m_c \cong 5.6$ for both the TE and TM modes, and the waveguide supports six TE modes and six TM modes, a total of twelve modes. On the other hand, we can maintain single-mode operation with a thinner film by increasing the refractive-index difference between the thin film and the substrate. The use of a high index contrast can therefore reduce the size of the waveguide and hence increase the level of device integration.

Electromagnetic theory. While the zig-zag wave model gives the correct equation, Eq. (5), for finding the effective indices of the guided modes, it does not lead to the field distributions. A rigorous analysis of the waveguide should be based on the electromagnetic theory. In what follows, the electric- and magnetic-field components in the p ($p = x, y$, or z) direction are denoted by E_p and H_p, respectively.

By applying Maxwell's source-free equations to a planar waveguide with an arbitrary refractive-index profile $n(x)$, the following wave equations can be derived (see, for example, reference 14):

$$\frac{d^2E_y}{dx^2} + [n^2(x)k^2 - \beta^2]E_y = 0 \tag{10}$$

for the TE mode, and

$$\frac{d}{dx}[\frac{1}{n^2(x)}\frac{dH_y}{dx}] + [k^2 - \frac{\beta^2}{n^2(x)}]H_y = 0 \tag{11}$$

for the TM mode. For the TE mode, $E_x = E_z = H_y = 0$ and H_x and H_z are related to E_y by

$$H_x = -\frac{\beta}{\omega\mu_0}E_y \tag{12}$$

and

$$H_z = -\frac{1}{j\omega\mu_0}\frac{dE_y}{dx}, \tag{13}$$

where μ_0 is the free-space permeability. Similarly, for the TM mode, $E_y = H_x = H_z = 0$ and E_x and E_z are related to H_y by

$$E_x = \frac{\beta}{\omega\varepsilon_0 n^2(x)}H_y \tag{14}$$

and

$$E_z = \frac{1}{j\omega\varepsilon_0 n^2(x)}\frac{dH_y}{dx}, \tag{15}$$

where ε_0 is the free-space permittivity. The problem is to solve for β and the field from the wave equation. There can be many sets of solutions, each set corresponding to a guided mode.

For a three-layer step-index slab waveguide, Eqs. (10) and (11) can be solved analytically. With reference to the coordinate system shown in Fig. 2, the field distribution that satisfies Eq. (10) or (11) can be written as

$$\psi(x) = \begin{cases} A\exp(W_3x/t), & -\infty < x < 0, \\ A\cos(Ux/t) + B\sin(Ux/t), & 0 \le x \le 2t, \\ (A\cos 2U + B\sin 2U)\exp[-W_2(x-2t)/t], & 2t < x < +\infty, \end{cases} \tag{16}$$

where $\psi = E_y$ for the TE mode, or $\psi = H_y$ for the TM mode. In Eq. (16), the normalized parameters U, W_2, and W_3 are defined by

$$U = kt[n_1^2 - (\beta/k)^2]^{1/2}, \tag{17}$$

$$W_2 = kt[(\beta/k)^2 - n_2^2]^{1/2}, \tag{18}$$

and

$$W_3 = kt[(\beta/k)^2 - n_3^2]^{1/2}. \tag{19}$$

It is clear from Eq. (16) that the spatial distribution of the field is sinusoidal within the film, while it decays exponentially in the cover and the substrate. The portions of the field that are localized in the cover and the substrate are referred to as the evanescent fields, which can carry a significant amount of power, especially when the mode is close to cut-off.

It is known from the electromagnetic theory that tangential electric and magnetic fields must be continuous at an interface between two different dielectric media. Equation (16) ensures that one of the tangential fields is continuous everywhere. For the TE mode, the continuity of the other tangential field H_z requires $d\psi/dx$ be continuous, while for the TM mode, the continuity of the tangential field E_z requires $[1/n^2(x)]d\psi/dx$ be continuous. By enforcing these boundary conditions at $x = 0$ and $x = 2t$, we obtain

$$B = r_3\frac{W_3}{U}A \tag{20}$$

and

$$\tan 2U = \frac{U(r_2W_2 + r_3W_3)}{U^2 - r_2r_3W_2W_3}, \tag{21}$$

where r_2 and r_3 are the same factors that appear in Eq. (6). With Eq. (20), the constant B can be eliminated from Eq. (16), which is then left with an arbitrary amplitude A. The propagation constants of the guided modes can be determined from Eq. (21), which is, in fact, identical to Eq. (5) obtained from the zig-zag wave model. With the knowledge of the propagation constants, the corresponding field distributions can be calculated from Eqs. (12)–(16). Figure 4 shows qualitatively the distributions of the electric-field components for several low-order TE and TM modes. The number of nulls (in the x direction) in the field distribution is simply equal to the mode order m. It should be noted that E_x, the dominant electric-field component for the TM mode, is discontinuous at the interfaces; it is $n^2(x)E_x$ that is continuous - see Eq. (14).

A guided mode carries optical power in the z direction. The power density (i.e., power per unit length in the y di-

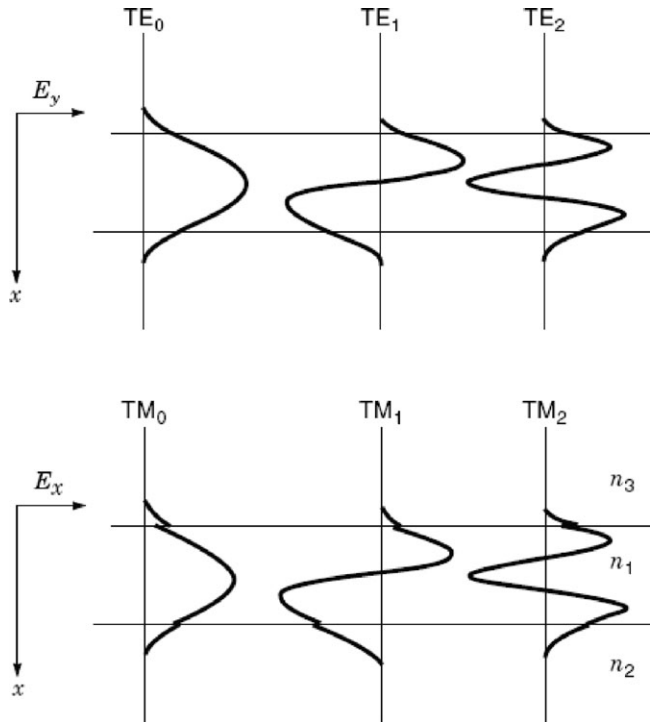

Figure 4. Field distributions for several low-order TE and TM modes of a step-index slab waveguide.

rection) can be calculated by integrating the z component of the Poynting vector in the x direction. The results are

$$P = \frac{\beta}{2\omega\mu_0}\int_{-\infty}^{+\infty} |E_y|^2\,dx \tag{22}$$

for the TE mode, and

$$P = \frac{\beta}{2\omega\varepsilon_0}\int_{-\infty}^{+\infty} \frac{|H_y|^2}{n^2(x)}\,dx \tag{23}$$

for the TM mode. By substituting Eq. (16) into the above expressions, the amplitude A in Eq. (16) can be expressed in terms of the power density P.

Dispersion curves. Equation (5) or (21), which is often called the dispersion relation or eigenvalue equation, allows us to calculate the dispersion characteristics of the guided mode, i.e., how the effective index β/k varies with the free-space wavenumber k. By scaling Eq. (5) with the normalized frequency V:

$$V = kt(n_1^2 - n_2^2)^{1/2}, \tag{24}$$

and the normalized propagation constant b:

$$b = \frac{(\beta/k)^2 - n_2^2}{n_1^2 - n_2^2}, \tag{25}$$

we obtain

$$2V(1-b)^{1/2} = m\pi + \tan^{-1}[r_2(\frac{b}{1-b})^{1/2}] + \tan^{-1}[r_3(\frac{b+a}{1-b})^{1/2}], \tag{26}$$

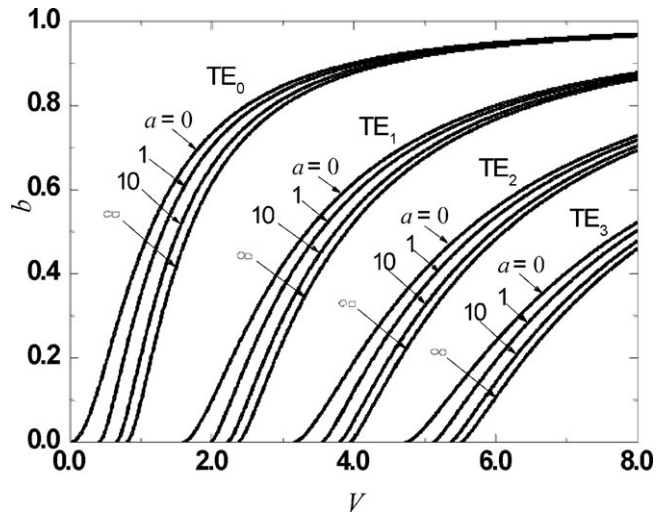

Figure 5. Universal dispersion curves for several low-order TE modes of a three-layer step-index slab waveguide.

where a is the asymmetry factor defined by Eq. (8). It can be seen that the normalized parameters are related by $V^2 = U^2 + W_2^2$ and $b = W_2^2/V^2$ $(0 < b < 1)$. By using the normalized parameters, the physical parameters of the waveguide no longer appear explicitly in the equation. The solutions can then be expressed as $b - V$ relations, which are universal in the sense that they are applicable to the entire class of waveguides. Figure 5 shows the universal dispersion curves for several low-order TE modes. By substituting $b = 0$ into Eq. (26), the cut-off value of V, denoted by V_c, can be determined:

$$V_c = \frac{1}{2}[m\pi + \tan^{-1}(r_3\sqrt{a})]. \tag{27}$$

In the case of a symmetric waveguide ($a = 0$), the TE_m and TM_m modes have the same cut-off V value $m(/2$, and there is no cut-off wavelength for the fundamental mode ($m = 0$).

Multilayer Waveguides

The approach outlined in the previous section can be applied to a waveguide that consists of more than three layers. The fields in the individual layers are first written down separately and the coefficients in the fields are then determined by the successive application of the boundary conditions at the interfaces. This procedure can in general lead to the dispersion relation. The form and the complexity of the solutions depend on how the fields are represented. A straightforward extension of the three-layer solutions has led to relatively simple dispersion relations for several four-layer and five-layer slab waveguides (4, 11). As the number of layers in the waveguide increases, the dispersion relation becomes more complicated. Nevertheless, compact dispersion relations in a recurrent form have been derived for general multilayer structures (18) and slab waveguide arrays (19). In the special case of a waveguide array with alternating high-index and low-index layers, the guided mode can be treated as a set of coupled zig-zag waves, which satisfy the transverse resonance conditions simultaneously (19).

Another approach to analyzing multilayer slab waveguides is based on modeling a multilayer waveguide with a stack of thin films, each of which is characterized by a two-by-two matrix that relates the reflected and transmitted fields (20). The characteristic matrix of the entire stack is given by the product of the individual matrices. By enforcing the condition that the fields decay exponentially in the first and the last layer, a dispersion relation in the form of a matrix equation results, from which the effective indices can be found by a root-searching technique.

Anisotropic Film Waveguides

Many active waveguide devices, such as electro-optic modulators and mode converters, rely on phase modulation of optical waves with applied electric fields. Such devices are usually built upon crystals with large electro-optic coefficients (such as lithium niobate and lithium tantalate), which possess anisotropic dielectric properties. An optically anisotropic crystal can be characterized by three principal refractive indices, which are associated with the principal axes of the crystal. When the three refractive indices have different values, it is called a biaxial crystal. When two of them are equal, it is called a uniaxial crystal. The actual refractive indices experienced by an optical wave propagating in the crystal depend on the direction in which the wave is launched into the crystal with respect to the principal axes of the crystal. In general, different electric-field components of the incident wave experience different refractive indices. This can give rise to the phenomenon of birefringence. In that case, the incident wave breaks up into two waves, which propagate independently in the crystal at different phase velocities.

When the principal axes of the materials that form the waveguide are arbitrarily oriented, TE and TM modes do not normally exist. The modes are, in general, hybrid in nature and it is a tedious exercise to find them (21). Fortunately, in most practical applications, the principal axes of the materials are aligned with the waveguide axes. In such special cases, the guided modes can still be classified as TE and TM modes and the simple zig-zag wave model described earlier can be extended to obtain the dispersion relation (22).

We refer to Fig. 2(a) for the geometry of the waveguide and, for generality, assume different anisotropic materials in different regions of the waveguide. The principal refractive indices are denoted by n_{ix}, n_{iy}, and n_{iz}, where $i = 1$ for the film, $i = 2$ for the substrate, and $i = 3$ for the cover. Because the TE mode possesses only an electric-field component in the y direction, it experiences only the refractive indices n_{iy}. The analysis for the TE mode is therefore the same as that in the isotropic case. The condition for the TE mode to exist is $n_{1y} > n_{2y}, n_{3y}$, and the dispersion relation is given by Eqs. (5) and (6) with n_1 and n_i replaced by n_{1y} and n_{iy}, respectively.

The analysis for the TM mode is slightly more complicated, owing to the fact that there exist two electric-field components. It can be shown (22) that the condition for the TM mode to exist is given by $n_{1x} > n_{2x}, n_{3x}$, and the dispersion relation for the TM mode obtained from the zig-zag wave model can be expressed as

$$2tkK_1[n_{1x}^2 - (\beta/k)^2]^{1/2} = m\pi + \Phi_2 + \Phi_3, \quad m = 0, 1, 2, \ldots, \tag{28}$$

with

$$\Phi_i = \tan^{-1}\{(\frac{n_{1z}}{n_{iz}})^2 \frac{K_i}{K_1} [\frac{(\beta/k)^2 - n_{ix}^2}{n_{1x}^2 - (\beta/k)^2}]^{1/2}\}, \quad i = 2 \text{ or } 3, \tag{29}$$

where $K_i = n_{iz}/n_{ix}$ $(i = 1, 2, 3)$ is a measure of the degree of anisotropy. For most anisotropic materials, K_i has a value between 0.8 and 1.2. Because of the material anisotropy, the effective indices for the TE and TM modes can be very different, and devices based on anisotropic waveguides can be highly sensitive to the polarization state of light. In fact, it is possible to design an anisotropic waveguide to support only one class of modes, and thus function as a waveguide polarizer or a mode filter (23).

Metal-Clad Waveguides

The three-layer structure shown in Fig. 2(a) becomes a metal-clad waveguide, when metal is employed as the cover material. At the optical frequency, the refractive index of metal is a complex number with a predominant negative imaginary part. For example, the refractive index of silver at the wavelength 0.633 μm is $0.0646 - j4.04$. Because of the complex nature of the refractive index, optical waves are attenuated when penetrating into the metal cover. The propagation constant for the guided mode is therefore also a complex number, where the real part is the phase constant and the (negative) imaginary part is the attenuation constant. The dispersion relation and the mode fields can be found by applying the electromagnetic theory to the waveguide in the same way as that described for the step-index slab waveguide (24, 25). In fact, the dispersion relation for the metal-clad waveguide is identical in form to that for the step-index slab waveguide (24); it is also given by Eqs. (5) and (6), provided that β and n_3 in these equations assume complex values. An important feature of the metal-clad waveguide is that it attenuates the TM_0 mode much more severely than the other modes. The attenuation constant for the TM_0 mode can be larger than that for the TE_0 mode by several orders of magnitude (25). This property has been explored for forming polarizers and mode filters.

Antiresonant Reflecting Optical Waveguides

In the conventional design of an optical waveguide, the refractive index of the guiding layer should be larger than that of the substrate to ensure light confinement without loss. For practical reasons, the substrate material may have a large refractive index. For example, the common substrate material silicon (Si) has a refractive index of 3.4–3.8, which is larger than the indices of most other waveguide materials. To form a low-loss waveguide on a high-index substrate, we may insert a sufficiently thick low-index buffer layer between the guiding layer and the substrate. In the case of using a Si substrate, a layer of SiO_2 (with a refractive index of (1.45) can be grown directly on Si by thermal oxidation. It is expensive, however, to produce a thick enough (> 4 μm) SiO_2 layer on Si. To overcome this problem, an interference cladding, which consists of

a properly designed high-index film deposited on a SiO_2 buffer layer, can be inserted between the guiding layer and the Si substrate to provide a large reflectivity (close to 100 %) at the operating wavelength of the waveguide. In this way, the SiO_2 buffer layer required can be relatively thin ($\sim 2\ \mu$m). Such a multilayer waveguide is known as an antiresonant reflecting optical waveguide (ARROW) (26). The dispersion relation of an ARROW can be cast in the same form as Eq. (5), except that the phase shift acquired at the interface between the guiding layer and the interference cladding, i.e., Φ_2 in Eq. (5), is obtained from the analysis of a multilayer structure (27).

Graded-Index Planar Waveguides

Several fabrication techniques, such as ion-diffusion and ion-exchange, can produce waveguides with refractive-index profiles that vary gradually in the transverse direction. Exact analytical solutions are available, however, only for a few symmetric refractive-index profiles, such as parabolic, sech-squared, and exponential profiles (4). More general profiles must be analyzed with either a numerical method or an approximate method. For a review of some numerical methods, see reference 11. In most practical cases, the refractive-index variation is smooth and slow, and the problem can be solved accurately with the WKB method (Wentzel-Kramers-Brillouin method), which is an approximate analytical method originally developed in quantum mechanics (28).

The WKB method. Figure 6 shows a graded-index profile $n(x)$, which decreases monotonically from the surface into the substrate with a peak index n_1 at $x = 0$. The index at infinity $n(+\infty)$ is equal to the substrate index n_2 and the index for $0 < x$ is equal to the cover (usually air) index n_3. Because the effective index of a guided mode must lie between n_1 and n_2, there must exist a location (turning point) in the x direction at which the effective index is equal to the refractive index of the profile, as shown by the point $x = x_t$ in Fig. 6. The idea of the WKB method is to assume an oscillatory field in the region $0 < x < x_t$, and an exponentially decaying field in the region $x_t < x < +\infty$. This assumption is accurate provided that the index variation is slow, compared with the optical wavelength.

To be specific, the field for a guided mode is expressed as

$$\psi(x) = \begin{cases} C_3 \exp(|q|x), & -\infty < x < 0, \\ (C_1/\sqrt{q})\cos(\int_0^x q\,dx - \Phi), & 0 \le x < x_t, \\ (C_2/\sqrt{|q|}\exp(-\int_{x_t}^x |q|\,dx)), & x_t < x < +\infty, \end{cases} \tag{30}$$

where

$$q(x) = [n^2(x)k^2 - \beta^2]^{1/2}. \tag{31}$$

For the TE mode, ψ and $d\psi/dx$ are continuous at $x = 0$, while for the TM mode, ψ and $[1/n^2(x)]d\psi/dx$ are continuous at $x = 0$. By enforcing these boundary conditions, we obtain

$$C_3 = \frac{r_3 \cos\Phi}{\sqrt{n_1^2k^2 - \beta^2}}\, C_1 \tag{32}$$

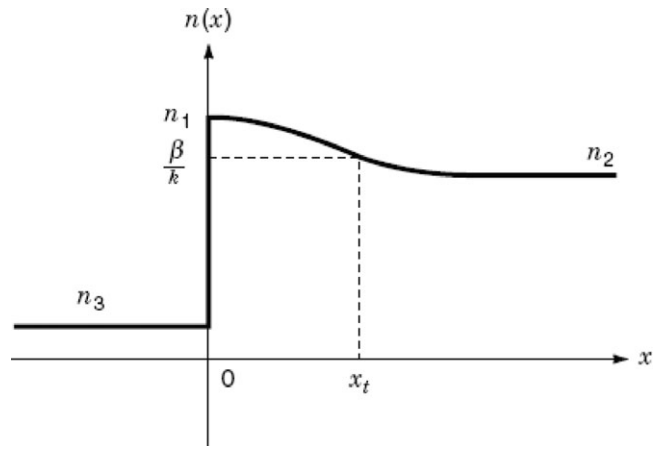

Figure 6. Refractive-index profile of a graded-index planar waveguide.

and

$$\Phi = \tan^{-1}\{r_3[\frac{(\beta/k)^2 - n_3^2}{n_1^2 - (\beta/k)^2}]^{1/2}\}, \tag{33}$$

where $r_3 = 1$ for the TE mode and $r_3 = (n_1/n_3)^2$ for the TM mode. As $q(x_t) = 0$, the approximation given by Eq. (30) fails at the turning point. To find the solution at $x = x_t$, the function $q^2(x)$ in the neighborhood of the turning point is approximated by a linear function:

$$q^2(x) = a_0^2(x - x_t) \tag{34}$$

where a_0^2 can be found from the slope of $n^2(x)$ at the turning point:

$$a_0^2 = k^2\frac{dn^2(x)}{dx}, \quad at\ x = x_t \tag{35}$$

With Eq. (34), the wave equation Eq. (10) or (11) has an exact solution:

$$\psi(x) = C_0 A_i(r) \tag{36}$$

where $A_i(r)$ is the Airy function (29) evaluated at $r(x)$ with $r(x) = -a_0^{-4/3}q^2(x)$. The solution given by Eq. (36) can be connected to those given by Eq. (30) in the regions $x > x_t$ and $x < x_t$ with the help of the asymptotic expressions for the Airy function in the respective regions (29). We thus find

$$C_2 = \frac{1}{2}C_1, \tag{37}$$

$$C_0 = \frac{\sqrt{\pi}}{a_0^{1/3}}C_1, \tag{38}$$

and the dispersion relation

$$k\int_0^{x_t}[n^2(x) - (\beta/k)^2]^{1/2}\,dx = m\pi + \frac{\pi}{4} + \Phi, \quad m = 0, 1, 2, \cdots. \tag{39}$$

After the effective index has been solved from Eq. (39), the corresponding mode field can be calculated from Eqs. (30)–(38).

Equation (39) has the same form as Eq. (5) and therefore can be interpreted by the zig-zag wave model. The left-hand

side of Eq. (39) represents the phase acquired by the zigzag wave in the guiding region ($0 < x < x_t$). The right-hand side implies that the wave acquires a (half) phase shift of $-\pi/4$ at the turning point, where total internal reflection takes place, and a (half) phase shift of $-\Phi$ at the surface. The phase shift Φ in Eq. (39) is in fact identical to the phase shift Φ_3 given by Eq. (6). Under the condition $n_1^2 - n_2^2 \ll n_1^2 - n_3^2$, it follows that $\Phi_3 \cong \pi 2$, regardless of the polarization of the wave. If the profile is of the buried type, i.e., $n(x)$ decreases monotonically in both the x and (x directions, the dispersion relation becomes

$$k\int_{x_1}^{x_2}[n^2(x)-(\beta/k)^2]^{1/2}\,dx=(m+\frac{1}{2})\pi,\quad m=0,1,2,\cdots, \tag{40}$$

where x_1 and x_2 are the turning points in the regions $x < 0$ and $x > 0$, respectively.

The accuracy of the WKB method has been investigated for a number of profiles (30). The method is more accurate for multimode waveguides. Nevertheless, it gives an adequate accuracy for many single-mode waveguides.

Some dispersion formulae. The refractive-index profile $n(x)$ shown in Fig. 6 can be written as

$$n^2(x)=n_2^2[1+2\Delta\ f(x/d)] \tag{41}$$

where d is a parameter characterizing the physical depth of the profile, Δ is the relative difference between the peak index and the substrate index, i.e., $\Delta=(n_1^2-n_2^2)/2n_2^2$, and $f(x/d)$ is a normalized function $0 \le f \le 1$ characterizing the shape of the profile. The effective index can also be written in a similar form:

$$(\beta/k)^2=n_2^2(1+2\Delta b) \tag{42}$$

where b is the normalized propagation constant defined by Eq. (25). The value of m at $b=0$, denoted by m_c, can be calculated by substituting Eqs. (41) and (42) into Eq. (39) (with $\Phi=\pi/2$) and setting $b=0$:

$$m_c=\frac{kdn_2(2\Delta)^{1/2}F}{\pi}-\frac{3}{4} \tag{43}$$

where

$$F=\int_0^{X_t} f(X)^{1/2}\,dX \tag{44}$$

with $X=x/d$. The number of modes supported by the waveguide is simply given by the next integer larger than m_c - see Eq. (9) for the case of a step-index waveguide. We can define a normalized mode order M ($0 \le M \le 1$) by (31)

$$M=\frac{m+\frac{3}{4}}{m_c+\frac{3}{4}}. \tag{45}$$

Putting Eqs. (41) and (42) into Eq. (39) (with $\Phi=\pi/2$) and using Eqs. (43) and (45), we obtain the normalized WKB equation:

$$\int_0^{X_t}[\ f(X)-b(M)]^{1/2}\,dX=FM \tag{46}$$

with $f(X_t)=b(M)$. For a given profile shape, the normalized propagation constant b depends only on the normalized mode order M. The $b-M$ relation applies to all guided modes. Table 1 shows the explicit dispersion formulae for some common profile shapes (31), which are obtained either by solving Eq. (46) analytically or by least-squares fitting numerical data with polynomials.

TWO-DIMENSIONAL WAVEGUIDES

In a planar waveguide, light is confined only in one transverse dimension and can diffract away in the other transverse dimension. To achieve a better control of the light wave and form devices that are compatible with optical fibers, light confinement in both transverse dimensions is necessary. All the waveguides shown in Fig. 1, except for the slab waveguide, can provide two-dimensional light confinement.

With the assumption that the wave propagates in the z direction with a propagation constantβ, the transverse electric field E_t in a two-dimensional waveguide with refractive-index distribution $n(x, y)$ satisfies the vector wave equation (32), which can be derived from Maxwell's source-free equations:

$$\nabla_t^2E_t+[n^2(x,y)k^2-\beta^2]E_t=-[E_t\cdot\frac{\nabla_t n^2(x,y)}{n^2(x,y)}], \tag{47}$$

where ∇_t is the transverse part of ∇. In general, the waveguide supports hybrid modes or vector modes, which contain all six field components. Once the transverse electric-field is found, the z component E_z and the magnetic field H can be calculated from

$$E_z=\frac{1}{j\beta}[\nabla_t\cdot E_t+E_t\cdot\nabla_t lnn^2(x,y)], \tag{48}$$

and

$$H=-\frac{1}{j\omega\mu_0}\nabla\times E. \tag{49}$$

Alternatively, one can first solve the transverse magnetic field from a wave equation similar to Eq. (47) and then find the other field components from Maxwell's equations.

Equation (47) actually consists of two equations coupling the x and y components of the electric field. When the index difference between the guiding region and the substrate is small, as in most practical cases, one of the two transverse field components becomes small (32) and the coupling terms in Eq. (47) can be ignored. This results in two independent quasi-vector wave equations (32):

$$\nabla_t^2E_x+[n^2(x,y)k^2-\beta^2]E_x=-\frac{\partial}{\partial x}[\frac{E_x}{n^2}\frac{\partial n^2}{\partial x}], \tag{50}$$

$$\nabla_t^2E_y+[n^2(x,y)k^2-\beta^2]E_y=-\frac{\partial}{\partial y}[\frac{E_y}{n^2}\frac{\partial n^2}{\partial y}], \tag{51}$$

which represent two different classes of modes. The modes governed by Eqs. (50) and (51) are linearly polarized and commonly referred to, respectively, as the E_{mn}^x and E_{mn}^y modes, where m and n are mode orders (integers ≥ 1), which specify the numbers of peaks in the field in the x and y directions, respectively. If the differentiation between the two polarizations is not important, the right-hand side of Eq. (47) can be dropped completely. This leads to the scalar

Table 1. Explicit dispersion formulae obtained from the WKB approximation (26) for some common profile shapes

Profile shape, $f(X)$	Profile volume, F	Dispersion formula, $b(M)$
Power-law:		
$\begin{cases} 1 - X^{\alpha}, & 0 \le X \le 1 \\ 0, & 1 \le X < +\infty \end{cases}$	$\int_0^1 (1 - X^{\alpha})^{1/2} dX$	$1 - M^{\alpha/(2+\alpha)}$
Sech-squared:		
$sech^2(X), \quad 0 \le X < +\infty$	$\pi/2$	$(1 - M)^2$
Tan-squared:		
$1 - \tan^2(\frac{\pi}{4} X), \quad 0 \le X < +\infty$	$2(\sqrt{2} - 1)$	$2 - [1 + (\sqrt{2} - 1)M]^2$
Gaussian:		
$\exp(-X^2), \quad 0 \le X < +\infty$	$\sqrt{\pi/2}$	$1.0000 - 1.6227M + 0.6817M^2$ $-0.3837M^3 + 0.3247M^4$
Error-function:		
$erfc(X), \quad 0 \le X < +\infty$	0.921915	$1.0000 - 0.5877M^{1/2} - 1.0819M$ $+0.1446M^{3/2} + 0.5250M^2$
Exponential:		
$\exp(-X), \quad 0 \le X + \infty$	2	$1.0000 - 0.8238M^{1/2} - 2.0870M$ $+2.6716M^{3/2} - 0.7608M^2$

wave equation:

$$\nabla_t^2 \psi + [n^2(x, y)k^2 - \beta^2]\psi = 0, \tag{52}$$

where ψ can represent any transverse field component. Under the scalar approximation, the E_{mn}^x and E_{mn}^y modes have the same propagation constant and field distribution. They are often called the scalar modes and can be denoted simply by the E_{mn} modes.

The problem of analyzing a two-dimensional waveguide is to solve Eq. (47), or Eqs. (50) and (51), or Eq. (52), depending on the level of accuracy required. It is in general more difficult to solve the full vector wave equation Eq. (47) than the other equations. Conventional numerical methods for boundary value problems, such as the finite element method and the finite difference method, can be employed to solve these equations. These methods are very versatile, as they can handle arbitrary geometries and refractive-index profiles, as well as anisotropic materials. Complications in applying these methods arise, however, in modeling the infinite open space with a finite number of elements or grid points, and in eliminating unphysical spurious solutions that may appear in solving the vector wave equation. There exists another class of numerical methods which are based on series expansion of the mode field. The point-matching method, the mode-matching method, the spectral-index method, and the Fourier-series expansion method are some of the popular ones. These methods are relatively easy to implement and particularly suitable for isotropic step-index waveguides. In addition to numerical methods, a number of approximate semi-analytical methods, such as Marcatili's method, the effective-index method, the perturbation method, and the variational method, are also available. They can give good results for certain waveguide structures. A survey of various numerical and approximate methods available for analyzing two-dimensional waveguides can be found in reference 32.

Rectangular-Core Waveguides

Rectangular-core waveguides are the most commonly used waveguide structures in integrated optics. Figure 7(a) shows the cross-section of a rectangular-core waveguide, where $2t$ and $2w$ are the thickness and the width of the core, respectively, and n_1, n_2, n_3, and n_4 are the refractive indices of the core and the surrounding claddings with $n_1 > n_2 \ge n_3, n_4$. In most practical cases, the index difference between the core and the substrate is small, i.e., $(n_1 - n_2)/n_1 \ll 1$. The structure shown in Fig. 7(a) represents several important classes of waveguides, including fully buried channel waveguides ($n_2 = n_3 = n_4$), embedded channel waveguides ($n_2 = n_4 < n_3$), and strip waveguides ($n_2 < n_3 = n_4$). Figure 7(b) shows qualitatively the field distributions of some low-order modes in a buried channel waveguide. Here we describe two popular approximate methods, namely, Marcatili's method (33) and the effective-index method (34), for the analysis of the waveguide shown in Fig. 7(a). Both methods solve approximately Eqs. (50) and (51) for the vector modes, or Eq. (52) for the scalar modes.

Marcatili's method. In the method proposed by Marcatili (33), the field in the rectangular-core waveguide is approximated by the product of the fields in two slab waveguides, which are obtained by extending the width and the height, respectively, of the rectangular-core waveguide to infinity, as shown in Fig. 8(a). To be specific, the field for the E_{mn}^y (E_{mn}^x) mode of the rectangular-core waveguide, ψ_{mn}, is ap-

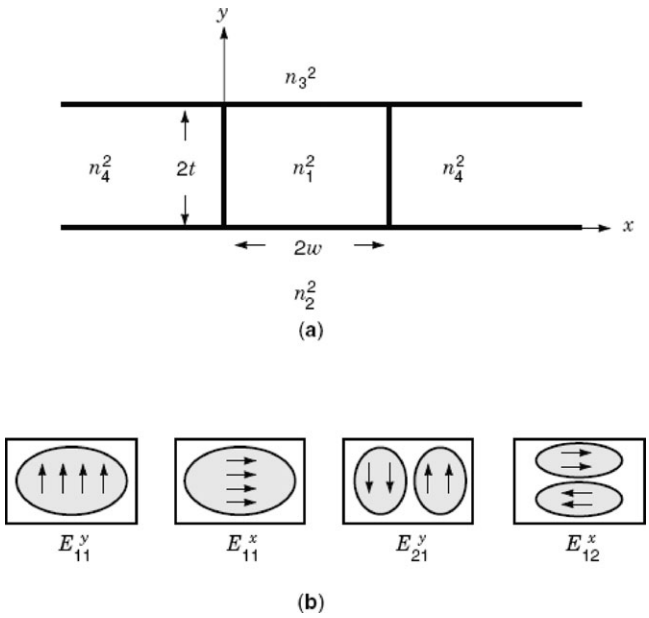

Figure 7. (a) Cross-sectional geometry of a rectangular-core waveguide, and (b) field patterns for several low-order modes, where the arrows represent the directions of the electric fields.

proximated by

$$\psi_{mn}(x, y) \cong \psi_m(x)\psi_n(y). \tag{53}$$

where ψ_m is the field for the TE_{m-1} (TE_{m-1}) mode of the slab waveguide with thickness $2w$, and ψ_{n-1} is the field for the TM_{n-1} (TE_{n-1}) mode of the slab waveguide with thickness $2t$. Here all the fields are transverse electric fields. In the case that the polarization effect is not taken into account, i.e., for the scalar modes, the TM mode can be replaced by the TE mode of the same order. The normalized propagation constant for the mode of the rectangular-core waveguide is simply given by

$$b = b_m + b_n - 1 \tag{54}$$

where $b_m = [(\beta_m/k)^2 - n_2^2]/(n_1^2 - n_2^2)$ and $b_n = [(\beta_n/k)^2 - n_2^2]/(n_1^2 - n_2^2)$ are the normalized propagation constants for the modes of the corresponding slab waveguides (with β_m and β_n the propagation constants). With this method, we only need to analyze two slab waveguides, or use the universal dispersion curves shown in Fig. 5 twice, to obtain an approximate solution for the rectangular-core waveguide.

It has been found that Marcatili's method actually solves a separable rectangular structure, as shown in Fig. 8(b) (35). This structure differs from the original waveguide shown in Fig. 7(a) in having lower refractive indices in the corner regions. Marcatili's method therefore always underestimates the propagation constant, and gives a poor accuracy in the near-to-cut-off regime, where the fields in the corner regions are significant. A correction factor for the propagation constant can be derived by treating the structure shown in Fig. 8(b) as a perturbation of the original structure shown in Fig. 7(a) (35).

The effective-index method. The idea of the effective-index method is to replace the rectangular-core waveguide

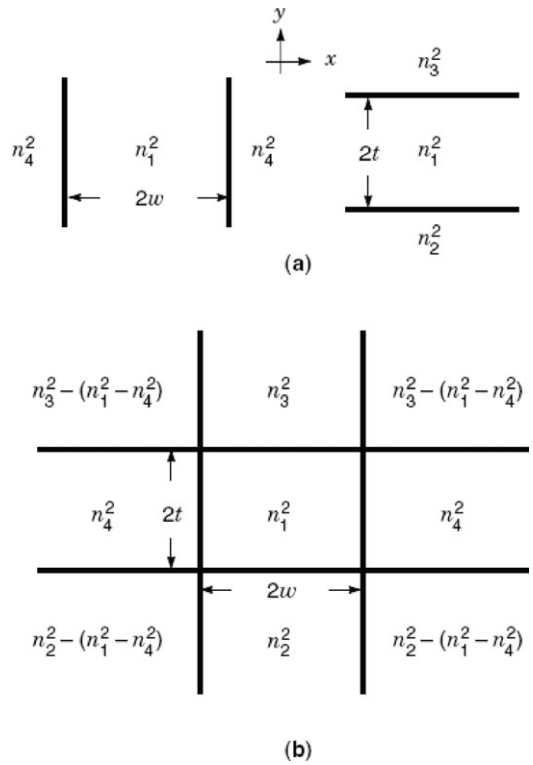

Figure 8. (a) In Marcatili's method, the rectangular-core waveguide in Fig. 7(a) is replaced by two slab waveguides. (b) The structure that is actually analyzed by the method differs from the original structure in having lower indices in the four corner regions.

by an equivalent slab waveguide with an effective refractive index obtained from another slab waveguide (34, 36). The effective-index method only requires solutions for two slab waveguides and is as efficient as Marcatili's method. The effective-index method is, however, more general, as it can be applied to a wide range of geometries and composite structures (36).

There are two ways of applying the effective-index method, depending on how the effective refractive index is calculated. In one method, as illustrated in Fig. 9(a), the mode index of the TM_{m-1} (TM_{m-1}) mode in the slab waveguide with thickness of $2t$ is used as the effective refractive index n_x of a second slab waveguide with thickness $2w$. The propagation constant of the TE_{n-1} (TM_{n-1}) mode of the second slab waveguide is regarded as the propagation constant of the E_{mn}^y (E_{mn}^x) mode of the rectangular-core waveguide. In the other method, as illustrated in Fig. 9(b), the mode index of the TE_{n-1} (TM_{n-1}) mode in the slab waveguide with thickness of $2w$ is used as the effective refractive index n_y of a second slab waveguide with thickness $2t$. The propagation constant of the TM_{m-1} (TE_{m-1}) mode of the second slab waveguide is the propagation constant of the E_{mn}^y (E_{mn}^x) mode of the rectangular-core waveguide. In both methods, the mode field in the rectangular-core waveguide is the product of the fields in the two slab waveguides. In the scalar analysis, the TM mode is replaced by the TE mode of the same order. The solutions obtained from the two methods for the same mode are in general different. The method that starts with a thinner slab usually gives a

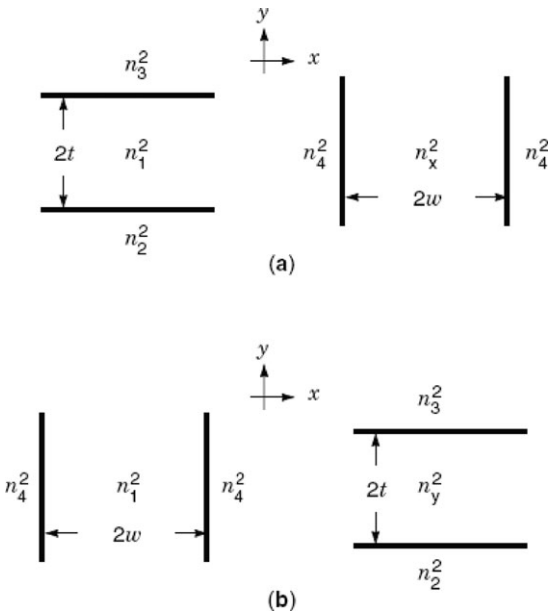

Figure 9. In the effective-index method, the rectangular-core waveguide in Fig. 7(a) is replaced by an equivalent slab waveguide, which has an effective index calculated from another slab waveguide. Two ways of applying the effective-index method are possible, depending on whether the slab waveguide with thickness (a) $2t$ or (b) $2w$ is used to determine the effective index.

better accuracy. By properly combining the solutions from the two methods, however, it is possible to derive a much more accurate solution (36).

The approximations involved in the effective-index method have been investigated for both the scalar (37) and vector (38) modes. Expressions for the errors in the method have been derived (37, 38), which show explicitly under what conditions the method is accurate. It can be shown that the method always overestimates the propagation constants for buried and embedded channel waveguides, but may underestimate the propagation constants for strip waveguides. The method shown in Fig. 9(a) is particularly accurate for strip waveguides.

Marcatili's method and the effective-index method are, in fact, special cases of a more general method (39). A generalization of the method shown in Fig. 9(a) is shown in Fig. 10, where a parameter γ is introduced in the claddings of the equivalent slab waveguide to differentiate between various methods. The conventional effective-index method corresponds to $\gamma = 0$, whereas Marcatili's method corresponds to $\gamma = 1$. It can be proved that a much better accuracy for the propagation constant can be obtained, if the following expression for γ is employed (40):

$$\gamma = 1 - \frac{(\Delta_4/\Delta_3)W_2 + (\Delta_4/\Delta_2)W_3}{2W_2W_3 + W_2 + W_3} \tag{55}$$

where $\Delta_i = (n_1^2 - n_i^2)/2n_1^2$ $(i = 2, 3, 4)$, and W_2 and W_3 are the normalized parameters for the slab waveguide with thickness $2t$. The method with γ given by Eq. (55) is called the effective-index method with built-in perturbation correction (39, 40).

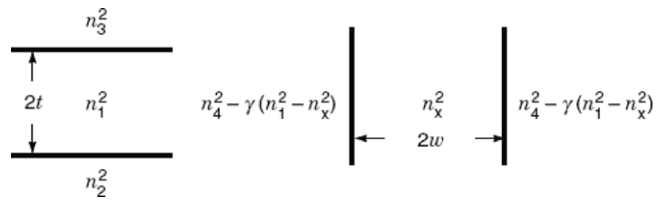

Figure 10. Same as in Fig. 9(a) except that the refractive index in the claddings of the equivalent slab waveguide is represented in a more general way.

Dispersion curves. Dispersion curves calculated by various methods for several low-order modes of a fully buried channel waveguide are shown in Fig. 11(a) for the case $w/t = 2$, and Fig. 11(b) for the case $w/t = 1$, where the normalized parameters are defined by $b = [(\beta/k)^2 - n_2^2]/(n_1^2 - n_2^2)$ and $V = kt(n_1^2 - n_2^2)^{1/2}$. The results obtained from Marcatili's method, the conventional effective-index method (starting with a thinner slab), Marcatili's method with perturbation correction (35), and the effective index with built-in perturbation correction (39) are compared. All these methods require the solutions of only two slab waveguides and, therefore, have the same degree of efficiency. Accurate numerical data calculated from a finite element method (41) are used as the references. Figure 11 shows clearly that the effective-index method with built-in perturbation correction is significantly more accurate than Marcatili's method and the conventional effective-index method, and slightly more accurate than Marcatili's method with perturbation correction. More numerical data for rectangular-core waveguides can be found in references 39 and 40. A rectangular-core waveguide can be designed to support only a number of E_{m1} modes by using a wide thin core. The propagation constants of these modes have approximately regular spacing and their interference gives rise to the effect of self-imaging, which forms the basis of a class of optical couplers, known as multimode interference (MMI) couplers (42).

Diffused Channel Waveguides

Diffused channel waveguides refer specifically to channel waveguides that are fabricated with the ion-diffusion technique. The refractive-index profile of a diffused channel waveguide can usually be described by a function that decreases monotonically in both the x and y directions in the substrate with a peak value at the surface of the waveguide. Many general numerical methods and approximate methods are available for analyzing such waveguides (32). Here we describe only the effective-index method (36, 43), which is particularly simple to implement.

Figure 12 shows how the effective-index method is applied to a diffused channel waveguide. The idea is to approximate the diffused channel waveguide by an equivalent planar waveguide with an effective index profile $n_e(x)$. As shown in Fig. 12, the effective index at a particular point $x = x_i$, i.e., $n_e(x_i)$, is given by the mode index calculated from the refractive-index profile of the diffused channel waveguide at $x = x_i$, i.e., $n(x_i, y)$, which varies only in the y direction. The propagation constant calculated for the profile $n_e(x)$ is treated as the approximate solution for

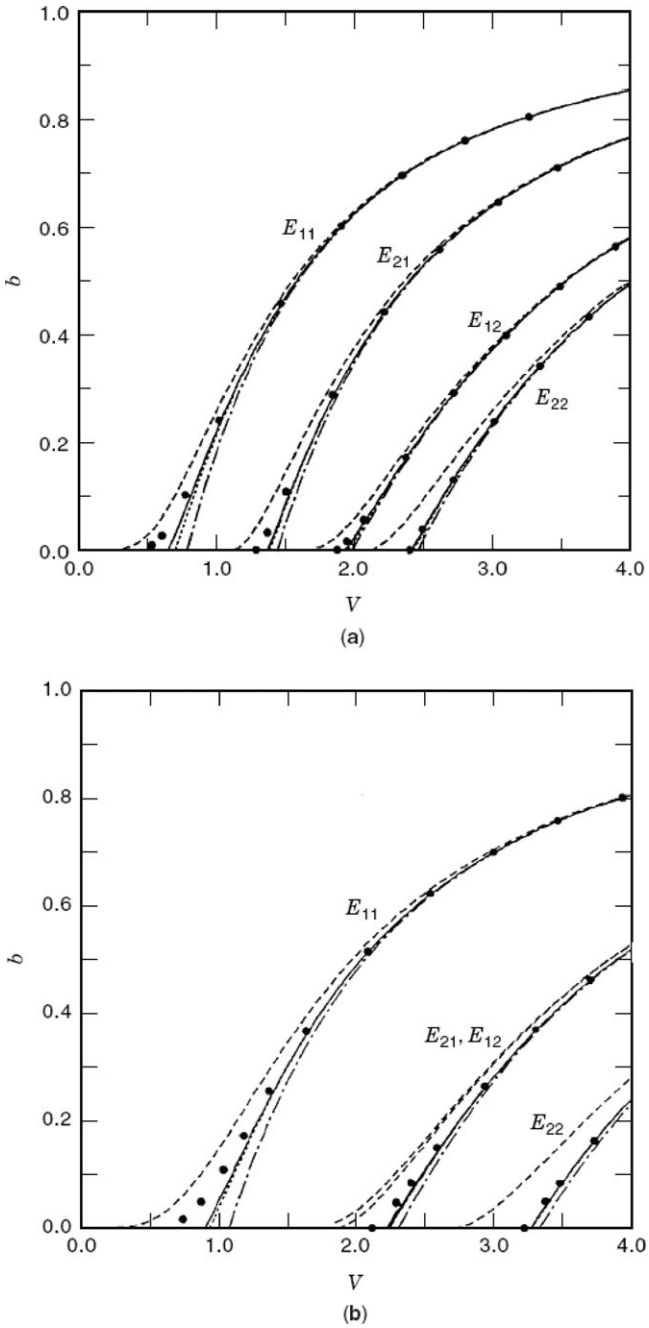

Figure 11. Universal dispersion curves for a buried channel waveguide calculated by various methods for (a) $w/t = 2$ and (b) $w/t = 1$: finite-element method (solid circles); conventional effective-index method (dashed curves); Marcatili's method (dot-dashed curves); Marcatili's method with perturbation correction (dotted curves); effective-index method with built-in perturbation correction (solid curves). (After Chiang (39). Reproduced by permission of the Institution of Electrical Engineers.)

the diffused channel waveguide. This method requires only the solutions for graded-index planar waveguides and is much more efficient than general two-dimensional numerical methods.

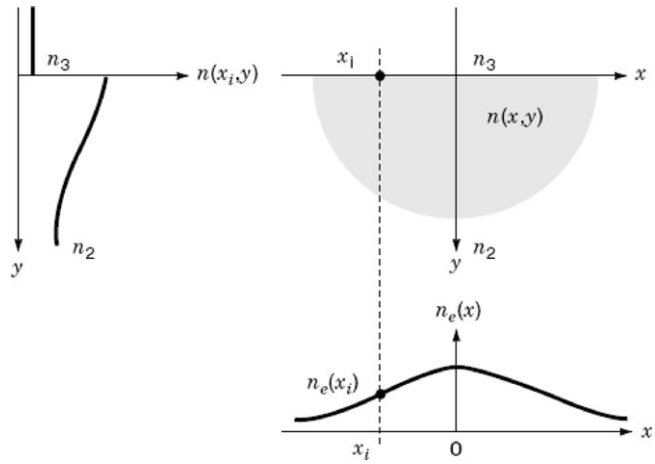

Figure 12. A diffused channel waveguide is replaced by an equivalent graded-index planar waveguide with refractive-index profile $n(x_i, y)$.

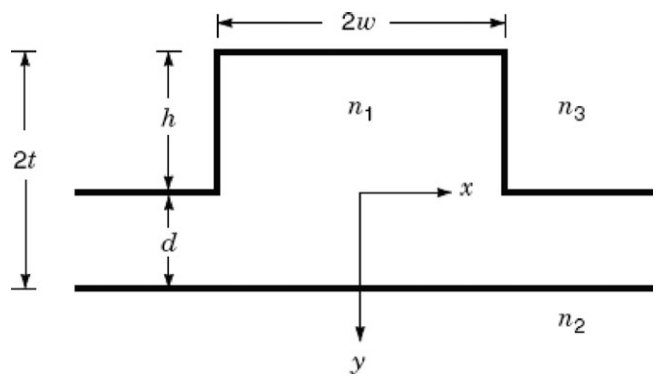

Figure 13. Cross-sectional geometry of a rib waveguide.

Rib Waveguides

Rib waveguide and its variations are common waveguide structures used in semiconductor-based optoelectronic devices. Figure 13 shows the geometry of a rib waveguide with width $2w$, rib-wall height h, and outer slab depth d. The thickness of the guiding region is $2t = h + d$. Technically, the effective-index method developed for rectangular-core waveguides can be applied to rib waveguides. With the effective-index method, the rib waveguide shown in Fig. 13 can be approximated by a symmetric three-layer slab waveguide with effective indices for the guiding layer and the claddings determined by the slab waveguides with thickness $2t$ and d, respectively. It is found, however, that the effective-index method is accurate only when the relative outer slab depth of the waveguide, $d/2t$, is either large or small (44). A preferred method for the analysis of rib waveguides is the spectral-index method (44).

The spectral-index method involves expanding the fields in the waveguide in terms of the local modes (modes of slab waveguides) and matching the fields along the base of the rib. The field matching, which is facilitated with a partial Fourier transform, can lead to a compact implicit dispersion relation. The spectral-index method can give good accuracy and requires much less computation time than general numerical methods. The details of the method as well

as its applications to more general rib structures are given in reference 44.

In the special case of a strip waveguide, i.e., $d = 0$, a perturbation analysis leads to an accurate explicit dispersion relation for the $d = 0$ mode ($p = x, y$) (45):

$$\beta_p^2 = {}^{a}\beta_p^2 - \frac{m^2\pi^2}{4w^2}[1 - \frac{2t}{wV}(\frac{\Delta_2}{\Delta_3})^{1/2}(1 - 2\Delta_3 S_p)], \qquad (56)$$

where $S_x = 1$, $S_y = 0$, $\Delta_i = (n_1^2 - n_i^2)/2n_1^2$ $(i = 2, 3)$, V is the normalized frequency defined by Eq. (24), and ${}^{a}\beta_p$ is the propagation constant of the TE_{n-1} ($p = x$) or TM_{n-1} ($p = y$) mode of the three-layer slab waveguide shown in Fig. 2. For the scalar (E_{mn}) mode, $S_p = 0$ and ${}^{a}\beta_x$ should be used. Equation (56) requires only the solution for a three-layer slab waveguide.

It can be proved from Eq. (56) that the propagation constants of the E_{mn}^x and E_{mn}^y modes can be made equal at a certain value of V by controlling the aspect ratio of the core, w/t (45). A single-mode waveguide with a polarization-independent propagation constant, namely, a zero-birefringence waveguide, is the building block of many polarization-insensitive devices where phase matching must be satisfied for both polarized modes. Zero-birefringence single-mode rib and strip waveguides have been demonstrated experimentally (46).

PHOTONIC BANDGAP WAVEGUIDES

Photonic bandgap (PBG) structures, also known as photonic crystals, are periodic structures that can take many different forms, such as multilayer stacks, arrays of holes in a single-material dielectric film or fiber, arrays of dielectric pillars, etc. (47). The most important feature of a PBG structure is the existence of forbidden frequency bands that prohibit light waves within these bands from propagating in the structure. Many of the applications with PBG structures are based on the destruction of their perfect periodic configurations by introduction of defects in the structures. The defects can be in the form of a layer of low-index film in the middle of a periodic multilayer stack, one or more missing or additional holes in a film or fiber filled with otherwise strictly regular holes, etc. While light within the forbidden bands cannot propagate in the perfect PBG structure, it can propagate through the defects with a low loss. Defect control in a PBG structure thus provides a highly effective means for the manipulation of light. A number of miniaturized optical components, wavelength filters, and lasers have been demonstrated with various kinds of PBG structures fabricated in different materials. The physical principles of different kinds of PBG structures are detailed in reference 47, while a comprehensive review of the technologies for the fabrication of PBG devices is given in reference 48. As PBG waveguides are the most basic structures used in PBG devices, we discuss a simple one-dimensional PBG waveguide as an example to illustrate the general dispersion properties of this class of waveguides.

Zig-Zag Wave Model

Figure 14 shows a one-dimensional PBG waveguide, where the guiding layer has refractive index n_g and thickness $2t$, and the claddings on both sides of the guiding layer are semi-infinite PBG structures made up of multilayer stacks of alternating refractive indices n_1 and n_2 with corresponding thicknesses t_1 and t_2. The structure is invariant in the y direction and light propagates in the z direction. The main feature of the PBG waveguide is that the guiding layer assumes a lower refractive index than its surrounding cladding (i.e., $n_g \le n_2 < n_1$). While the principle of total internal reflection does not apply to the PBG waveguide, light guidance in such a waveguide can be understood from the fact that, within the forbidden bands of the PBG structures, light undergoes complete reflection and can be trapped in the guiding layer, regardless of its low index. The guiding layer acts as a defect in the infinite periodic structure. Therefore, light propagation in the PBG waveguide can be described as plane waves bouncing back and forth along the waveguide as in the case of a conventional slab waveguide.

With the zig-zag wave model, the dispersion relation of the PBG waveguide can be expressed in the form of the transverse resonance condition as

$$2tk[n_g^2 - (\beta/k)^2]^{1/2} = m\pi + 2\Phi, \quad m = 0, 1, 2, \ldots, \qquad (57)$$

where k is the free-space wavenumber, β is the propagation constant, and -2Φ is the phase shift acquired when the wave is incident upon the boundary between the guiding layer and the infinite PBG structure. Equation (57) has the same form as Eq. (5). For a conventional three-layer slab waveguide, the phase shift at the boundary is derived from the condition of total internal reflection, as given by Eq. (6), and the range of the effective index β/k (and hence the range of the incidence angle θ) is small. For the PBG waveguide, however, the phase shift -2Φ is a characteristic of the PBG structure, which is derivable from a transfer-matrix method (49). The range of the effective index is given by $0 \le \beta/k \le n_g$, which is large. The upper bound ($\beta/k = n_g$) corresponds to grazing incidence ($\theta = \pi/2$), while the lower bound ($\beta/k = 0$) corresponds to normal incidence ($\theta = 0$), which suggests that the effective index can be much smaller than the refractive index of the material.

Dispersion Curves

To facilitate discussion, we define the normalized frequency V as

$$V = k\Lambda(n_1^2 - n_2^2)^{1/2}, \qquad (58)$$

and the normalized propagation constant b as

$$b = \frac{(\beta/k)^2 - n_2^2}{n_1^2 - n_2^2}, \qquad (59)$$

where $\Lambda = t_1 + t_2$ is the pitch of the periodic structure. The dispersion characteristics of the waveguide are expressed as the relationship between b and V (the $b - V$ curves). Here, V is defined in terms of the parameters of only the PBG structure, so that the dispersion curves for all the waveguides, regardless of their thicknesses and refractive indices, can be compared with reference to the same band diagrams of the PBG structure. For the sake of simplicity, we assume $n_g = n_2$. For a guided mode, the condition $0 \le \beta/k \le n_2$ is translated into $1/(1 - r_{12}) \le b \le 0$, where $r_{12} =$

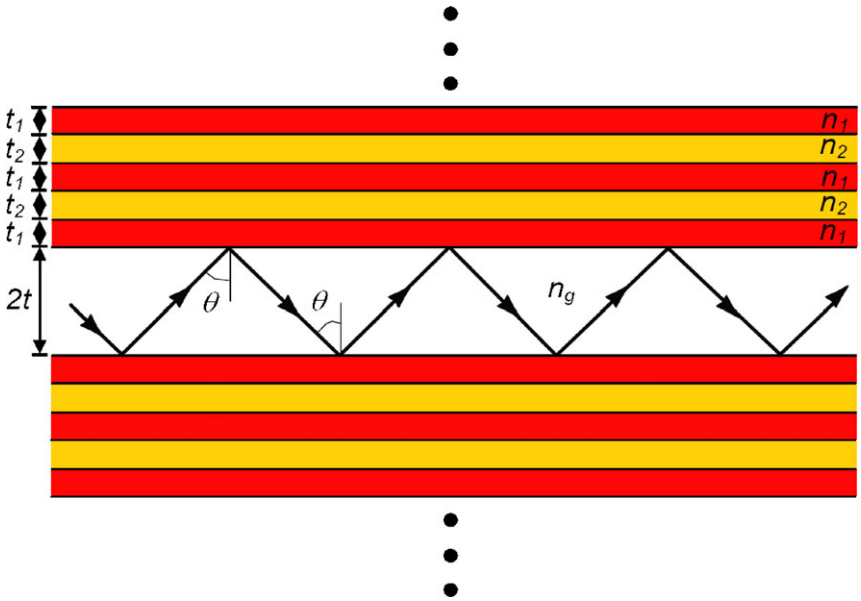

Figure 14. A one-dimensional photonic bandgap (PBG) waveguide formed by sandwiching a low-index layer (film) between two identical semi-infinite periodic slab structures.

$(n_1/n_2)^2$. The dispersion curves of the TE modes are actually independent of r_{12}, so there is no need to specify the value of r_{12} for the calculation of their dispersion curves. The dispersion curves of the TM modes, however, depend on the value of r_{12}.

As an example, we set $t_1 = t_2$, $t = \Lambda$, and $r_{12} = 2.25$. The dispersion curves for the TE and TM modes are shown in Fig. 15(a) and Fig. 15(b), respectively, where the shaded areas are the forbidden bands of the PBG structure. Each forbidden band is labeled by a band order n (= 1, 2, 3,. . .). Within each band, the mode is labeled by a mode order m, the integer that appears in Eq. (57). A comparison of Fig. 15 and Fig. 5 shows that the dispersion characteristics of the PBG waveguide are distinctly different from those of a conventional slab waveguide. Apart from the difference in the range of the effective index, the dispersion curves of the PBG waveguide are fragmentary. As shown in Fig. 15, many dispersion curves have the same mode order m, but they are not connected because of the presence of band gaps. These curves terminate at the band edges at which the modes are at cut-off. It is therefore possible to operate the waveguide at a suitable value of V, so that the higher-order modes instead of the lower-order modes are supported.

The dispersion curves of the TM modes show some additional features. As shown in Fig. 15(b), there exist two special lines, the B-line and the L-line. The B-line specifies Brewster incidence at which the effective index is given by $\beta/k = n_1 n_2/(n_1^2 + n_2^2)^{1/2}$ or $b = 1/(1 - r_{12}^2) = -0.246$. Under this condition, light can pass through the PBG structure without decaying (49). The forbidden bands shrink to points along the B-line. The L-line specifies the minimum value of b that is allowed, i.e., $b = 1/(1 - r_{12}) = -0.8$, which corresponds to $\beta/k = 0$. A comparison of Fig. 15(a) and Fig. 15(b) shows that the TM bands fall completely within the TE bands. In the analysis of omnidirectional reflection of the PBG structure, only the TM forbidden bands need to be considered (50). A careful inspection of the labels of the curves in Fig. 15 shows some missing mode orders (for

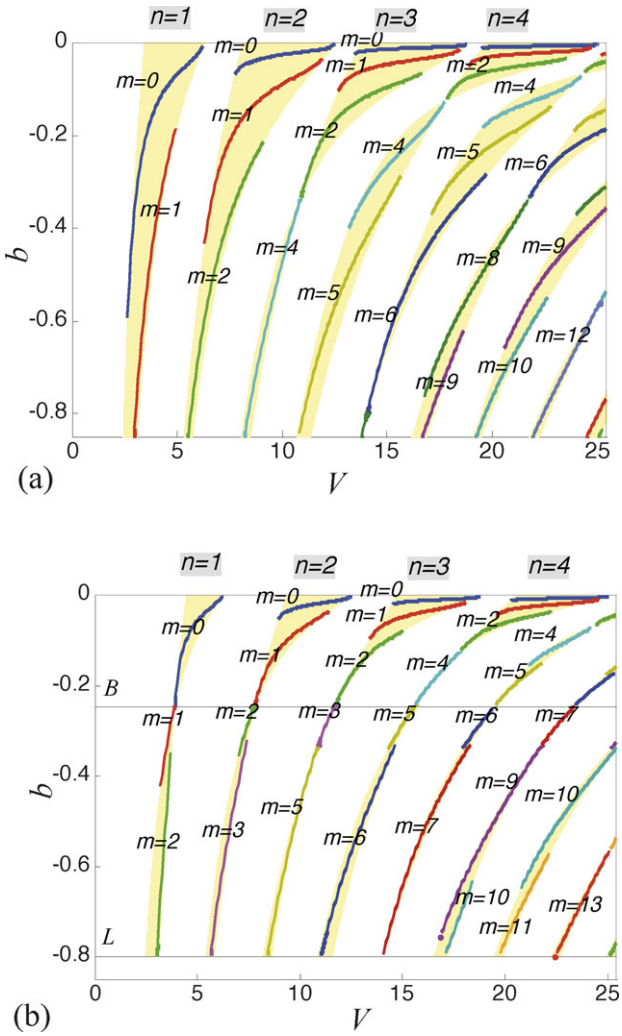

Figure 15. Universal dispersion curves for a one-dimensional PBG waveguide with $n_g = n_2$, $t_1 = t_2$, $t = \Lambda$, and $r_{12} = 2.25$ for (a) the TE modes and (b) the TM modes.

example, m = 3 and 7 for the TE modes). These missing modes do not exist because their dispersion curves shrink into points together with the forbidden bands (not due to Brewster incidence).

As discussed earlier, each of the guided modes can be labeled uniquely with the mode order m and the band order n. In fact, these mode orders allow the field patterns of the guided modes to be visualized intuitively. The electric field of the TE mode, i.e., $E_y(x)$, contains m + 1 peaks in the guiding layer and n zero crossings in each period of the PBG structure. The magnetic field of the TM mode, i.e., $H_y(x)$, contains m + 1 peaks in the guiding layer above the B-line while m zero crossings in the guiding layer below the B-line, and n zero crossings in each period of the PBG structure.

It should be mentioned that the guiding layer of the PBG waveguide can have a refractive index larger than that of the surrounding PBG structure. In that case, forbidden bands still exist but the band gaps can become much narrower.

Two-dimensional PBG waveguides such as one that has a low-index rectangular core surrounded by periodic cladding structures can be converted approximately into one-dimensional PBG waveguides by the effective-index method in the same way as depicted in Fig. 8 and Fig. 9. Analysis of more general PBG structures that involve index variations along the z direction (e.g., structures that contain arrays of air holes in the wave propagation direction) usually requires a purely numerical approach based on a propagation method, such as the finite-difference time-domain method (51).

DIRECTIONAL COUPLERS

When two parallel waveguides are placed in close proximity to each other, a directional coupler is formed. Under appropriate conditions, light launched into one of the waveguides can couple completely into the neighbor waveguide. Directional couplers are used widely in optical communication systems and integrated optical circuits as power dividers, wavelength multiplexers/demultiplexers, and polarization splitters. In this section, we describe two commonly used methods for analyzing directional couplers, with a coupler consisting of two parallel identical step-index slab waveguides as an example. A more rigorous treatment of directional couplers can be found in reference 12.

Normal-Mode Analysis

Figure 16(a) shows two parallel identical three-layer step-index slab waveguides, where $2t$ and n_1 are the thickness and the index of the guiding slabs, respectively, n_2 is the index of the surrounding medium, and $2d$ is the separation between the two waveguides. In the normal-mode analysis, the directional coupler is treated as a composite waveguide, i.e., a five-layer step-index slab waveguide in the present example. The composite waveguide supports two classes of modes: the even modes, which have symmetric field distributions, and the odd modes, which have antisymmetric field distributions. The field distributions for the lowest-order even and odd TE modes are also shown in Fig. 16(a).

For the sake of simplicity, we assume that the composite waveguide supports only the lowest-order even and odd modes. When light is launched into only one of the guiding slabs, these two modes are simultaneously excited and each carries approximately half of the input power. This can be seen by superposition of the two mode fields shown in Fig. 16(a), which results in a total field localized in only one guiding slab. Because the two modes propagate at different phase velocities, they acquire a phase difference as they propagate along the coupler. The phase difference acquired increases with the distance and is given by $(\beta_+ - \beta_-)z$, where β_+ and β_- are the propagation constants for the even and odd modes, respectively. We can assume that the two modes are in phase when they are excited at z = 0. After propagating a distance $z = L_c$ given by

$$L_c = \frac{\pi}{\beta_+ - \beta_-}, \tag{60}$$

the two modes become 180 degree out of phase. A superposition of the two mode fields then produces a total field localized in the opposite guiding slab, i.e., the optical power is transferred to the opposite guiding slab. In fact, the optical power is transferred back and forth between the two guiding slabs at every L_c. The behavior of a directional coupler is therefore characterized by $L_c$or $\beta_+ - \beta_- \equiv 2C$. L_c and C are commonly referred to as the coupling length and the coupling coefficient, respectively.

To calculate L_c or C, we must find β_+ and β_-. Using the method outlined in the previous section for analyzing a three-layer slab waveguide, we obtain the following dispersion relations for the five-layer slab waveguide:

$$\tan 2U = \frac{r_2 U W_2[1 + \tanh(W_2 d/t)]}{U^2 - r_2^2 W_2^2 \tanh(W_2 d/t)} \tag{61}$$

for the even modes, and

$$\tan 2U = \frac{r_2 U W_2[1 + \coth(W_2 d/t)]}{U^2 - r_2^2 W_2^2 \coth(W_2 d/t)} \tag{62}$$

for the odd modes, where $r_2 = 1$ for the TE mode and $r_2 = (n_1/n_2)^2$ for the TM mode, and U and W_2 are given by Eqs. (17) and (18), respectively. The propagation constants β_+ and β_- can be solved exactly from Eqs. (61) and (62), respectively, by a root-searching technique.

Coupled-Mode Analysis

The normal-mode analysis just described relies on the knowledge of the modes of the composite waveguide. Except for very simple structures, exact solutions for such modes are difficult to find. A more practical approach to analyzing directional couplers, especially when complicated waveguide geometries are involved, is based on the coupled-mode theory (14), which requires only the solutions of the modes of the individual waveguides that form the coupler.

In the coupled-mode theory, the modes of the composite waveguide are approximated by the modes of the individual waveguides in isolation. For the coupler shown in Fig. 16(a), the fields of the lowest-order even and odd modes, $\psi_+(x)$ and $\psi_-(x)$, can be expressed, respectively, as

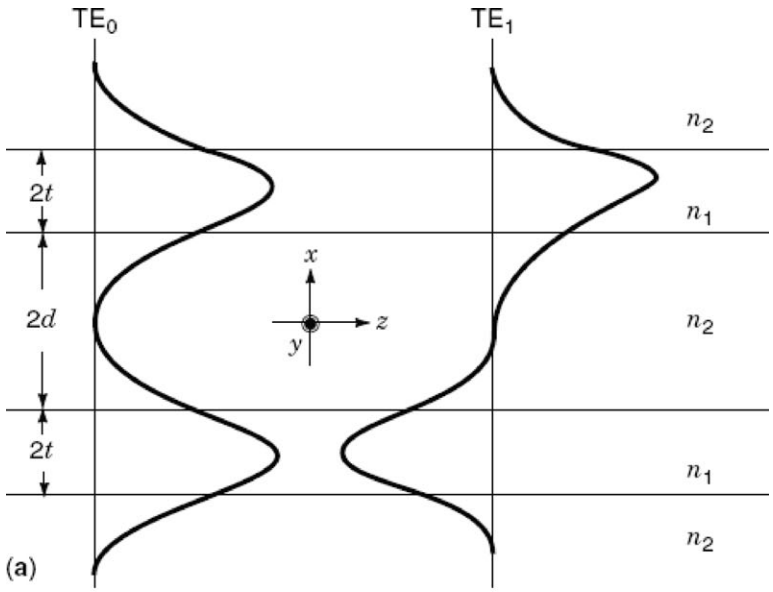

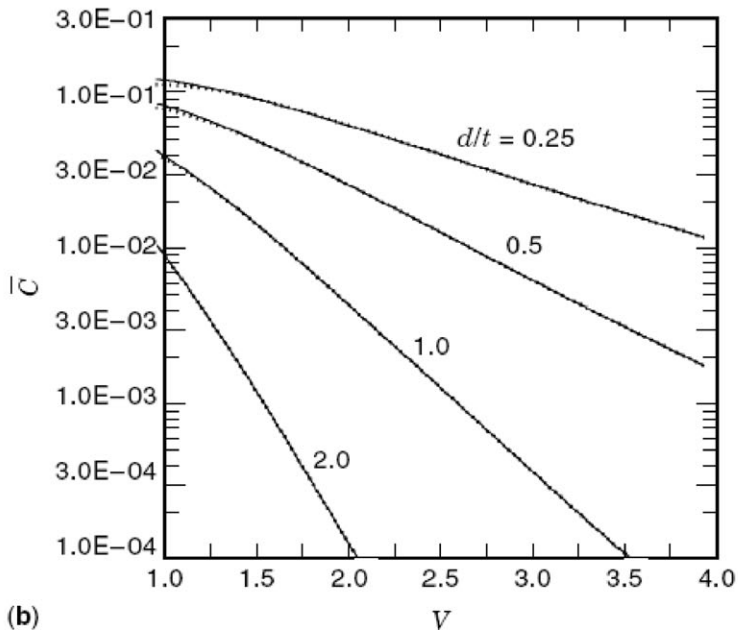

Figure 16. (a) Geometry of a directional coupler consisting of two parallel identical three-layer slab waveguides together with the field distributions for the two lowest-order TE modes of the composite five-layer waveguide structure. (b) The normalized coupling coefficient of a directional coupler decreases rapidly with increasing the normalized frequency and the relative waveguide separation. Numerical results are obtained for the coupler in (a) from the normal-mode theory (solid curves) and the coupled-mode theory (dotted curves).

the sum and the difference of the fields in the three-layer slab waveguides that form the coupler:

$$\psi_{\pm}(x) \cong \psi(x-d-t) \pm \psi(x+d+t), \tag{63}$$

where $\psi(x)$ is the field of the fundamental mode of the three-layer slab waveguide. For the sake of simplicity, we consider only the TE mode. By substituting Eq. (63) into the TE wave equation, Eq. (10), and integrating the resultant equation over the entire x domain, we find

$$\beta_{\pm}^2 \cong \beta^2 \pm k^2(n_1^2 - n_2^2)\frac{\int_{d+t}^{d+2t} \psi(x-d-t)\psi(x+d+t)dx}{\int_{-\infty}^{+\infty} \psi(x)^2 dx}, \tag{64}$$

where β is the propagation constant for the TE_0 mode of the three-layer slab waveguide. The overlap integral in Eq. (64) measures the degree of overlapping between the mode fields in the two waveguides over the guiding region of one of the waveguides. Equation (64) involves only the solutions for the fundamental mode of a single waveguide. Using the solutions for the three-layer slab waveguide, we obtain:

$$\beta_+^2 - \beta_-^2 \cong \frac{2V^2}{t^2}\frac{B}{N} \tag{65}$$

with

$$B = \frac{2W_2}{V^2}\exp(-W_2\frac{2d}{t}) \tag{66}$$

and

$$N = \frac{V^2}{U^2} + \frac{W_2}{U^2} + \frac{1}{W_2}, \tag{67}$$

where the normalized parameters are defined for the three-layer slab waveguide – Eqs. (17), (18) and (24). It should be noted that the accuracy of the assumption Eq. (63), and hence, the coupled-mode solution Eq. (64), increases with the normalized waveguide separation d/t and the normalized frequency V.

Figure 16(b) shows the normalized coupling coefficient $\overline{C}$ as a function of V for several values of relative waveguide separation d/t, where $\overline{C} \equiv 0.25V[(\beta_+/k)^2 - (\beta_-/k)^2]/(n_1^2 - n_2^2)$. Results obtained from the normal-mode analysis and the coupled-mode analysis are hardly distinguishable, except when both d/t and V are small. As shown in Fig. 16(b), the normalized coupling coefficient decreases rapidly as the normalized frequency and the relative waveguide separation increase. As an example, with $2t = 2\ \mu$m, $n_1 = 2.20$, $n_1^2 - n_2^2 = 0.02n_1^2$, we have $V = 1.5$ at the wavelength 1.3 μm. When the waveguide separation is equal to the thickness of the guiding slabs ($2d = 2\ \mu$m), the coupling length is approximately 0.7 mm. If we double the waveguide separation ($2d = 4\ \mu$m), the coupling length will increase by roughly ten times, to approximately 8 mm.

The coupled-mode theory also leads to simple expressions to describe power evolution in the individual waveguides. When the two waveguides are identical and lossless and optical power is launched into only one of the waveguides at $z = 0$, the powers in the two waveguides, denoted by $P_1(z)$ and $P_2(z)$, respectively, are given by

$$P_1(z) = P_\mathrm{i} \cos^2(Cz) \tag{68}$$

and

$$P_2(z) = P_\mathrm{i} \sin^2(Cz), \tag{69}$$

where P_i is the input power. These expressions are consistent with our earlier discussion with the normal-mode analysis that a complete transfer of optical power from one waveguide to the other takes place over a coupling length, i.e., at $z = L_c = \pi/2C$. When the length of the coupler is chosen to be equal to an odd multiple of $L_c/2$. The coupler functions as a power divider with a 50/50 splitting ratio (i.e., a 3-dB coupler), which distributes optical power equally between the two waveguides. In principle, any splitting ratio can be achieved by choosing a suitable length. It is also possible to design a coupler that functions as a wavelength multiplexer or demultiplexer, by making use of the fact that the coupling coefficient C depends on the wavelength. When the length of the coupler is equal to an even number of coupling lengths at one wavelength, and an odd number of coupling lengths at the other wavelength, the two wavelengths of light, both launched into one of the waveguides, can evolve separately from the two waveguides. Similarly, a polarization splitter can also be realized with a directional coupler, if the coupling coefficient is sensitive to the polarization state of light.

A directional coupler can also be formed with two dissimilar waveguides. In general, a complete transfer of optical power cannot take place in such an asymmetric coupler at all wavelengths. However, it is possible to design an asymmetric coupler that allows a complete power transfer at a specific wavelength, and hence, serves as a wavelength filter.

Although we detail only the analysis of two parallel slab waveguides, the underlined principles apply to general waveguide geometries. In fact, the results obtained for parallel slab waveguides can be readily extended to directional couplers consisting of parallel rectangular-core waveguides by means of the effective-index method (52). Directional couplers with polarization-insensitive splitting ratios, which are formed with rectangular-core waveguides, have been demonstrated experimentally (53).

As shown by the results in Fig. 16(b), evanescent-field coupling between two waveguide cores is effective only when the two cores are sufficiently close to each other. For widely separated cores where evanescent-field coupling is negligible, we can still achieve strong light coupling between the cores by introduction of properly designed periodic structures (i.e., gratings) along the cores (54).

FABRICATION TECHNIQUES

Techniques commonly used in fabricating optical waveguides can be divided into three categories, according to how the guiding layer of the waveguide is formed. The three categories are (i) deposition, in which material is deposited in the form of thin film on a lower-index substrate; (ii) ion-migration, in which ions are introduced into a substrate to raise the refractive index of the substrate near the surface; and (iii) epitaxial growth, in which a layer of crystallized material is grown epitaxially on a similar substrate material. In general, deposition and epitaxial techniques lead to step-index waveguides, while ion-migration techniques give rise to graded-index waveguides. A fabrication technique could be applied to many different material systems, while waveguides based on the same material system could be fabricated with more than one technique. Table 2 shows some typical waveguide materials together with the more commonly used fabrication techniques. More detailed discussions on waveguide fabrication can be found in the relevant chapters in the reference books (3,7,9,10,13,55).

Deposition Techniques

Sputtering is the most versatile deposition method and allows deposition of glass or crystalline films on glass substrates as well as on crystalline substrates. In the sputtering process, atoms from a solid target material are made to eject in a vacuum by the bombardment with atoms or ions, and the ejected particles are collected on a nearby substrate to form a thin film. In the glow-discharge sputtering method, the ions used for bombardment are generated from a plasma, which is formed by ionizing an inert gas (e.g. argon) with a high voltage (several kilovolts) applied to the target (which serves as the cathode). For a metal target, a dc voltage is applied (dc sputtering), while for a dielectric target, a radio-frequency (RF) voltage is used (RF sputtering) to prevent accumulation of positive ions at the target, which could counteract the applied voltage and stop the process. Alternatively, high-speed ions can be generated with an ion gun instead of a glow-discharge plasma (ion-beam sputtering). Ion-beam sputtering can allow a better control of the substrate temperature and the physical parameters in the deposition process. It is also possible to al-

Table 2. Some common waveguide materials and fabrication techniques

Material	Refractive index	Type of waveguide	Fabrication technique
Glasses	1.45 – 1.55	Step-index	RF sputtering
		Graded-index	Ion-exchange
Polymers	1.45 – 1.65	Step-index	Spin-coating
			Polymerization
$LiNbO_3$	$n_o = 2.29, n_e = 2.20$	Graded-index	Metal in-diffusion
	(at λ = 0.633 μm)		Proton-exchange
ZnO	2.0 (at λ = 0.633 μm)	Step-index	RF sputtering
Silicon on insulator (SOI)	3.47/1.46 (at λ = 1.55 μm)	Step-index	PECVD
SiO_xN_y on silica	1.46 – 2.0	Step-Index Graded-index	PECVD
Chalcogenide	2 – 3	Step-index	Thermal vapor deposition
$Ga_{1-x}Al_xAs$	3.4 – 3.6	Step-index	Epitaxial growth
$Ga_{1-x}In_xAs_{1-y}P_y$	3.2 – 3.6	Step-index	Epitaxial growth

low oxygen to react with a metal target during deposition to form a metal oxide film at the substrate surface (reactive sputtering). In general, sputtering provides pure, durable, and low-loss films, but the deposition rate is usually low (of the order of 0.01 – 0.1 μm per minute).

For the deposition of polymers, the spin-coating and dip-coating methods can be used. A substrate is first covered with, or dipped into, a liquid of polymer solution. The thickness of the liquid layer is then controlled by either spinning the substrate at an appropriate rate (spin-coating) or by lifting it up vertically to allow excess liquid to run off (dip-coating). The film is subsequently dried in air and baked in an oven. This method is simple and capable of producing low-loss waveguides, but it is difficult to control the film thickness and uniformity to a high accuracy. A more elaborate method for producing polymer thin films is called plasma polymerization, which involves the use of an electrical discharge to convert a monomer (low molecular weight organic compound) chemically into a smooth polymer film. This method provides a much better control of the film thickness.

Other deposition techniques include thermal vapor deposition and chemical vapor deposition. In the former, a thin film is formed by depositing a material vaporized in a vacuum chamber on a substrate, while in the latter, thin-film deposition is the result of chemical reactions of gases. Chemical vapor deposition is a common method for making silica-based waveguides. In fact, it is a standard method for making optical fiber preforms. The thin-film deposition process can be enhanced at lower temperatures by using a vapor that contains electrically charged particles (plasma). This technique is known as plasma enhanced chemical vapor deposition (PECVD). It is widely employed for the fabrication of high-index-contrast waveguides based on silicon-on-insulator (SOI) or silicon oxynitride (SiO_xN_y) on silica (56).

Ion-Migration Techniques

In the thermal diffusion method, a metal film is deposited on a substrate and heated at a high temperature (around 1000 °C) for a period of several hours. The metal is then diffused into the substrate and a smooth graded-index profile near the surface of the substrate is formed. An electric field may be applied during the diffusion process to accelerate the process and reduce the temperature required (electric-field assisted diffusion). The electric field can also drive the diffused ions well below the surface of the substrate to produce a buried waveguide and eliminate surface scattering. Titanium-diffused lithium niobate (Ti:LiNbO) waveguides and copper-diffused lithium tantalate (Cu:$LiTaO_3$) waveguides are well-known examples of waveguides fabricated with thermal diffusion.

In the ion-exchange method, a substrate is immersed in a molten salt at a suitable temperature (200 – 350 °C) for a period of time. The ions in the substrate are then exchanged with the ions in the molten salt. This process in general results in a gradual change in the refractive index near the surface of the substrate. In some cases, the ion-exchange process can be accelerated by applying an electric field (electric-field assisted ion-exchange). For example, glass waveguides can be made by exchanging sodium ions in glass with silver, potassium, or thallium ions. A detailed description of the ion-exchange method for a wide range of glass waveguides can be found in reference 55. In the special case that metal ions in a crystalline substrate are exchanged with hydrogen ions (protons) from an acid, the method is called the proton-exchange method. The proton-exchange method can usually lead to a relatively large refractive-index change and a step-like profile. For example, a lithium niobate waveguide can be made by exchanging lithium ions with protons in a solution of benzoic acid at around 250 °C. The process may take a few minutes for a single-mode waveguide to many hours for a heavily moded waveguide.

Graded-index waveguides can also be fabricated with the ion-implantation technique, in which a stream of accelerated ions are made to penetrate into a substrate material and, consequently, cause lattice disorder, and hence, index change in the material. This technique is expensive to implement, but it can be applied to a wide range of materials and provide an accurate control of the waveguide parameters.

Epitaxial Techniques

Epitaxial techniques are widely used for the fabrication of semiconductor waveguides. The principle of epitaxial growth is that a material in its molten state (liquid-phase epitaxy) or gaseous state (vapor-phase epitaxy) can be crystallized into thin films on the surface of a substrate material, when the two materials have similar crystal struc-

tures and lattice constants. In vapor-phase epitaxy, chemical reactions of gases take place at a high temperature. In general, epitaxial techniques can produce high-quality crystalline films with well-controlled thicknesses. It is also possible to grow crystalline thin films by allowing beams of atoms or molecules from different sources to react with a crystalline substrate under ultrahigh vacuum conditions (molecular-beam epitaxy). Molecular-beam epitaxy offers good flexibility and an extremely precise control of film thickness (layers as thin as 1 nm can be grown).

Patterning

The fabrication techniques described above only lead to planar waveguides. To make a two-dimensional waveguide, it is necessary to carry out patterning, either on a planar waveguides or on a substrate.

Figure 17(a) shows the main steps involved in fabricating a two-dimensional waveguide on a planar waveguide. The planar waveguide is first coated with a layer of (negative) photoresist followed by a metal mask with a window with the desired dimension. The strip of photoresist in the window, after exposure to ultraviolet light, is developed chemically, and remains to serve as a protective shadow on the planar waveguide. The guiding layers of the waveguide that are not covered by the photoresist mask are then removed with an etching technique. If the etching is complete (down to the substrate), a strip waveguide results. If the etching is incomplete, a rib waveguide results.

It is also possible to make a two-dimensional waveguide from a substrate material, as shown in Fig. 17(b). The substrate material is coated directly with a layer of positive photoresist and a metal mask. After exposure and development, in contrast with the previous case, the photoresist that has been exposed to ultraviolet light is removed chemically. This leaves a window of photoresist on the substrate. A layer of higher-index material is then sputtered on the patterned structure. In this way, only a strip of higher-index material is in touch of the substrate. With the rest of the photoresist removed, a strip waveguide results. A diffused channel waveguide is formed instead, if a layer of metal for thermal diffusion is deposited on the patterned structure, so that diffusion takes place only in the window area. When a lower-index layer is further deposited on a strip or embedded waveguide, a fully buried channel waveguide results.

Two patterning techniques are available: photolithography, in which photoresists are used, as described in the examples, and electron-beam lithography, in which electron-beam resists are used. With the electron beam technique, patterns are written directly on the resists by the electron beam and no mask is required. A typical resolution of 0.1 μm can be achieved. There are also two kinds of etching techniques: "wet" etching techniques, which rely on liquid chemicals as etching agents, and "dry" etching techniques, which rely on gaseous chemicals. Dry etching usually results in better etched surfaces. Reactive ion etching (RIE) is a particularly versatile dry-etching technqiue, where high-energy ions generated under low pressure or in vacuum by an electromagnetic field are made to attack the substrate and react with it to remove the material.

There are two other general techniques that are particularly suitable for the fabrication of polymer waveguide devices: laser direct writing and imprinting/molding (57).

Laser writing is based on changing the refractive index of photosensitive polymer by exposing it to a laser beam of a suitable wavelength. Waveguide patterns can be produced directly on a polymer substrate with a computer-controlled moving laser beam or an expanded stationery laser beam through a mask. When a polymer that is insensitive to the writing wavelength is used as the cladding material, it is possible to form buried waveguides directly (58). The laser writing technique can also be applied to the fabrication of embedded waveguides in photosensitive glass (59).

The imprinting/molding technique is most suitable for mass production of polymer waveguides. This technique requires the preparation of a mold or stamp that contains the device pattern. There are several versions of the technique. In the case of imprinting, the mold or stamp is made in conformal contact with the polymer film coated on a substrate to transfer the pattern. In the case of hot embossing, the mold is pressed against a polymer film at an elevated temperature and peeled off from the film by cooling. It is also common to fill the mold with the desired polymer in the liquid form followed by ultra-violet curing. The advantage of the imprinting/molding technique is that the mold can be used repeatedly to produce the same device with a simple process and thus lower the manufacturing cost. The mold can be produced directly by photolithography on silicon or glass. More often the mold is made of a mechanically flexible elastomer poly(dimethysiloxane) (PDMS) (see, for example, reference 60), which is produced by casting from a master. The master to be replicated can be made of commonly used resist, glass, or semiconductor.

CHARACTERIZATION AND MEASUREMENTS

After a waveguide has been fabricated, the next step is to measure its properties. The results from the measurements can provide valuable information about how good the fabrication technique is, and how well the fabricated waveguide meets the design specifications. It is through a number of iterations of fabrication and measurement that a reproducible fabrication method can be established for a specific type of waveguide. The properties of a waveguide that are of particular interest are optical attenuation, refractive-index profile, and, in the case of a single-mode waveguide, mode-field distribution. More detailed discussions of various measurement methods can be found in the relevant chapters of the reference books (3,7,10,13,55).

Prism-Coupling Technique

Essentially all optical measurements involve launching light into a waveguide. Here the prism-coupling technique (61) is described briefly, which is widely used in waveguide characterization.

Figure 18 shows a prism with base angle α_p and refractive index n_p, placed against the surface of a planar waveguide with a small air gap. A collimated light beam is incident upon the prism at an angle θ and deflected onto the base of the prism at an angle θ' to the normal of the base.

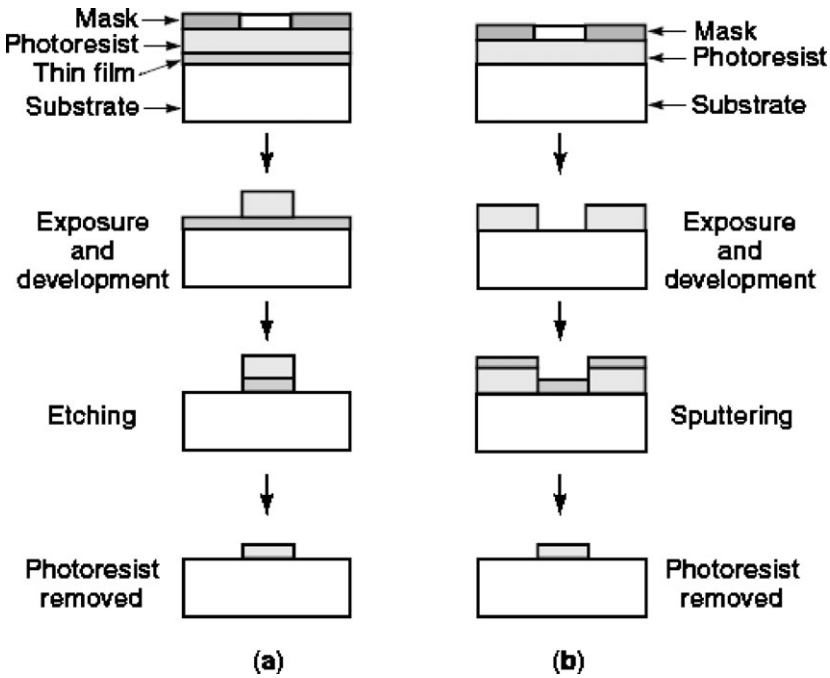

Figure 17. Procedures in the fabrication of a strip waveguide starting with (a) a step-index slab waveguide or (b) a substrate.

It can be shown that, only when the phase velocity of the incident beam along the base of the prism is equal to the phase velocity of the guided mode of the waveguide, light can be coupled into that mode with a high efficiency (61). This condition leads to

$$\frac{\beta}{k} = n_{\mathrm{p}} \sin\theta' = n_{\mathrm{p}} \sin[\sin^{-1}(\sin\frac{\theta}{n_{\mathrm{p}}}) + \alpha_{\mathrm{p}}] \tag{70}$$

where β/k is the effective index of the mode. For the method to work properly, the refractive index of the prism must be sufficiently larger than that of the guiding layer of the waveguide. It is clear from Eq. (70) that, by varying the incident angle θ, any guided mode can be selectively excited. This method is capable of providing a high coupling efficiency (better than 80 %). To obtain a stable and efficient coupling condition, however, the adjustment of the gap separation and beam position is critical. Exactly the same method can be used to couple light out of the waveguide.

The other commonly used method for launching light into a waveguide is the end-coupling (end-fire) method, in which light is launched into the waveguide through the end face of the waveguide. This method requires the end face of the waveguide be flat and perpendicular to the input light beam.

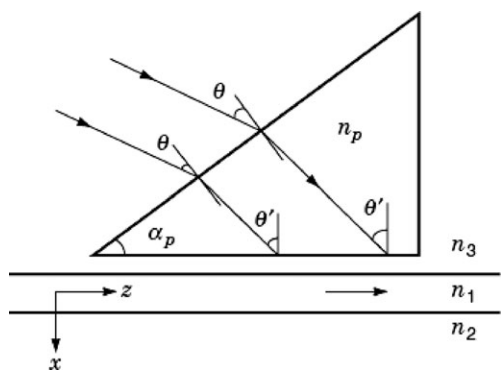

Figure 18. Illustration of the prism-coupling technique. A high-index prism is placed against the surface of a planar waveguide and light is launched into the waveguide through the prism. Only when the phase velocity of the incident light along the base of the prism is equal to that of a guided mode of the waveguide, the mode can be excited with a high efficiency.

Loss Measurements

A high-quality waveguide should have a low optical loss (typically less than 1 dB/cm). There are two kinds of losses: absorption loss caused by light absorption in the waveguide materials, and scattering loss caused by the imperfections in the waveguide structure. Absorption loss is an important concern in semiconductor waveguides, as there are many mechanisms in semiconductors that can cause absorption (interband absorption, impurity absorption, and carrier absorption). On the other hand, scattering loss is the major loss in many dielectric waveguides. In general, waveguides fabricated from diffusion techniques have a lower scattering loss. For curved waveguides, there also exists bend-induced radiation loss.

In general, the optical loss in a waveguide, denoted by α (in dB/cm), can be calculated from optical power levels P_1 and P_2 measured respectively at two different positions z_1 and z_2 in the waveguide:

$$\alpha = \frac{10\log(P_1/P_2)}{z_1 - z_2}. \tag{71}$$

To measure power levels at two different positions, the cutback method can be used. Light is launched into the waveguide by the end-coupling technique and the output power at the other end of the waveguide is measured. The waveguide is then cut by a known length and the same measurement is repeated to obtain another power reading. This method is accurate, but destructive. An alternative method is based

on the use of two prisms, one for launching light into the waveguide and the other for coupling light out of the waveguide. The output prism is allowed to slide along the waveguide and couple light out of the waveguide at different locations. In this way, output power levels at different positions can be measured. The prism-sliding technique is non-destructive and capable of measuring loss for individual mode. However, care must be taken to ensure that the coupling efficiency is optimized, and hence, remains constant during the measurement. This can be facilitated by filling the air gap between the prism and the waveguide with an index-matching liquid. The use of index-matching liquid can improve the coupling efficiency and reduce the friction. Measurements of losses down to ~0.1 dB/cm with errors of ±0.01 dB/cm are possible with this method. The scattering loss in a waveguide can also be measured by detecting light scattered from the waveguide with an optical fiber probe or a camera placed near the surface of the waveguide.

Refractive-Index Profile Measurements

In the case of using prisms to couple light into and out of a waveguide, if the light incident upon the input prism spans a range of angles, all the guided modes of the waveguide can be excited and leave from the output prism at different angles. The output pattern displayed on a screen shows a number of parallel bright lines ("m-lines"), each of which represents a guided mode (2, 61). By measuring the exit angles of the modes, the effective indices can be calculated from Eq. (70). The prism-coupling method thus provides a convenient way for measuring mode indices. With the knowledge of the effective indices, the thickness and the refractive index of the thin film in a step-index waveguide can be determined from Eq. (5). As there are two unknowns, at least two effective indices are required.

In the case of a graded-index waveguide, the refractive-index profile can be determined from the inverse WKB method. A common way of applying the inverse WKB method is to treat the effective index in the WKB equation, Eq. (39), as a continuous function of m (the effective-index function) (62), i.e., $N(m) \equiv \beta/k$, where m is a real number instead of an integer. According to Eq. (39), there exists a one-to-one correspondence between the refractive-index profile $n(x)$ and the effective-index function $N(m)$. The idea is therefore to find approximately the function $N(m)$ from a set of discrete effective indices ($m = 0, 1, 2, \ldots$) measured by the prism-coupling method. This can be done by plotting the measured effective indices against the mode orders and then least-squares fitting the data to generate a continuous function of m (with a low-order polynomial). From Eq. (39), by extrapolating $N(m)$ to $m = -0.75$, the peak index at the waveguide surface can be obtained, i.e., $n_1 = N(-0.75)$. To facilitate the calculation, the function $N(m)$ is replaced by a large number of samples N_i ($i = 0, 1, 2, \ldots$) with $N_0 > N_1 > N_2 > \ldots$ and $N_0 = N(-0.75) = n_1$, each of which corresponds to a turning point x_i at which $n(x_i) = N_i$. The turning points can then be calculated from the following algorithm (62):

$$x_i = \frac{(m+0.25)\pi + \Phi(N_i) - k\sum_{j=1}^{i-1}\{x_j[(\overline{N}_j^2 - N_i^2)^{1/2} - (\overline{N}_{j+1}^2 - N_i^2)^{1/2}]\}}{k(\overline{N}_2^i - N_i^2)^{1/2}} \quad (72)$$

for $i = 2, 3, \cdots$ with $x_0 = 0$ and $x_1 = [(m_1 + 0.25)\pi + \Phi(N_1)]/[k(\overline{N}_1^2 - N_1^2)^{1/2}]$, and $\overline{N}_i = (N_i + N_{i-1})/2$. Once the turning points are found, the refractive-index profile $n(x)$ can be constructed. In general, the accuracy of the method increases with the number of effective indices available for forming the effective-index function. In the original version of the method (62), at least three effective indices from the same mode type (TE or TM) are required, which means that the waveguide must support at least three modes of the same type. By combining the measurements for both the TE and TM modes and/or at different wavelengths, the method can be applied to single-mode and two-mode waveguides (63). However, the technique of combining the measurements for both mode types cannot be applied to waveguides that do not support both mode types or contain unknown material birefringence, while the technique of combining the measurements at different wavelengths requires several laser sources and an accurate knowledge of the dispersion properties of the waveguide material. These problems can be overcome with the technique that combines the effective indices of the same mode measured with different index-matching liquids applied to the surface of the waveguide (64).

Mode-Field Distribution

To optimize the coupling efficiency between a single-mode fiber and a single-mode waveguide, the mode-field distributions in the fiber and the waveguide must match. The mode-field distribution in a waveguide, or the near-field intensity pattern, can be measured conveniently with a video camera system. In fact, the measured near-field intensity pattern can be used to determine the refractive-index profile of the waveguide. From Eq. (52), the refractive-index profile $n(x, y)$ can be calculated from (65)

$$n^2(x, y) = (\frac{\beta}{k})^2 - \frac{1}{2k^2 I}[\nabla_t^2 I - \frac{1}{2I}(\nabla_t I)^2] \quad (73)$$

where $I(x, y) \propto \psi^2(x, y)$ is the near-field intensity pattern. Because numerical calculation of first and second derivatives on the measured data is involved, very accurate experimental data are required and data smoothing is necessary. This method is capable of determining refractive-index profiles in two-dimensional waveguides.

CONCLUDING REMARKS

With continuous research endeavors for almost four decades, numerous integrated optical devices have been demonstrated, varying from simple ones, which may function merely as passive signal distributors, to complicated ones, which may involve a complicated matrix of waveguides and a large number of thermal controls. Indeed, the advancement in waveguide fabrication over the years has greatly improved the control of waveguide dimensions and made possible the launch of a range of products at reasonable prices. For example, silica-waveguide star couplers and high-speed $LiNbO_3$ modulators are among the most

common integrated optic waveguide devices in the market. Commercial software packages are also available for the design of a wide range of waveguide devices.

The continuing pursue for higher transmission capacity with optical fiber has brought about the concept of dense wavelength-division multiplexing (DWDM), which demands the transmission of a large number of closely packed wavelength channels along a single-mode fiber. The most important enabler of the DWDM technology is the integrated optic device known as the arrayed-waveguide grating (AWG). An AWG consists of a large array of waveguides with a fixed length difference between two neighboring waveguides, where the light outputs from all the waveguides are made to interfere to provide spatial separations for a large number of DWDM channels. An AWG thus fulfils the key function in the DWDM technology as a wavelength multiplexer/demultiplexer. A comprehensive review of the AWG technology can be found in chapter 9 of reference 17. At the same time, the rapid advances in the waveguide fabrication techniques allow further miniaturization of optical waveguides by using high-index-contrast structures, in particular, silicon-based structures (56). The recent developments in photonic crystals, which are also high-index-contrast structures, have opened up many new opportunities in the realization of compact devices (48) and the application of nonlinear optical phenomenon (66). On the other hand, polymer waveguides hold promise for mass production of low-cost and high-performance devices for the next generation of optical communication systems (57–68). More exciting developments along these fronts are expected to come with time.

BIBLIOGRAPHY

1. S. E. Miller, Integrated optics - an introduction, *Bell Syst. Tech. J.*, **48**, 2059–2068, 1969.
2. P. K. Tien, Integrated optics and new wave phenomena in optical waveguides, *Reviews of Modern Physics*, **49**, 361–420, 1977.
3. H. Nishihara, M. Haruna, and T. Suhara, *Optical Integrated Circuits*, New York: McGraw-Hill, 1989.
4. T. Tamir (ed.), *Guided-Wave Optoelectronics*, 2nd ed., Berlin: Springer-Verlag, 1990.
5. R. Syms and J. Cozens, *Optical Guided Waves and Devices*, London: McGraw-Hill, 1992.
6. K. J. Ebeling, *Integrated Optoelectronics*, Berlin: Springer-Verlag, 1993.
7. S. Martellucci, A. N. Chester, andM. Bertolotti (ed.), *Advances in Integrated Optics*, New York: Plenum Press, 1994.
8. T. P. Lee (ed.), *Current Trends in Integrated Optoelectronics*, Singapore: World Scientific, 1994.
9. E. J. Murphy (ed.), *Integrated Optical Circuits and Components: Design and Applications*, New York: Marcel Dekker, 1999.
10. R. G. Hunsperger, *Integrated Optics: Theory and Technology*, 5th ed., Berlin: Springer-Verlag, 2002.
11. M. J. Adams, *An Introduction to Optical Waveguides*, New York: Wiley, 1981.
12. A. W. Snyder and J. D. Love, *Optical Waveguide Theory*, London: Chapman and Hall, 1983.
13. D. L. Lee, *Electromagnetic Principles of Integrated Optics*, New York: Wiley, 1986.
14. D. Marcuse, *Theory of Dielectric Optical Waveguides*, 2nd ed., San Diego: Academic Press, 1991.
15. K. Kawano, *Introduction to Optical Waveguide Analysis: Solving Maxwell's Equations and the Schrödinger Equation*, New York: John Wiley & Sons, 2001.
16. G. Lifante, *Integrated Photonics: Fundamentals*, New York: John Wiley & Sons, 2003.
17. K. Okamoto, *Fundamentals of Optical Waveguides*, 2nd ed., San Diego: Academic Press, 2006.
18. Y.-F. Li and J. W. Y. Lit, General formulas for the guiding properties of a multilayer slab waveguide, *J. Opt. Soc. Amer. A*, **4**, 671–677, 1987.
19. K. S. Chiang, Coupled-zigzag-wave theory for guided waves in slab waveguide arrays, *J. Lightwave Technol.*, **10**, 1380–1387, 1992.
20. L. M. Walpita, Solutions for planar waveguide equations by selecting zero elements in a characteristic matrix, *J. Opt. Soc. Amer. A*, **2**, 595–602, 1985.
21. T. A. Maldonado and T. K. Gaylord, Hybrid guided modes in biaxial planar waveguides, *J. Lightwave Technol.*, **14**, 486–499, 1996.
22. V. Ramaswamy, Propagation in asymmetrical anisotropic film waveguides, *Appl. Opt.*, **13**, 1363–1371, 1974.
23. P. Sosnowski, Polarization mode filters for integrated optics, *Optics Commun.*, **4**, 408–412, 1972.
24. S. C. Rashleigh, Four-layer metal-clad thin film optical waveguides, *Opt. Quantum Electron.*, **8**, 49–60, 1976.
25. I. P. Kaminow, W. L. Mammel, and H. P. Weber, Metal-clad optical waveguides: analytical and experimental study, *Appl. Opt.*, **13**, 396–405, 1974.
26. M. A. Duguay, Y. Kokubun, T. L. Koch, and L. Pfeiffer, Antiresonant reflecting optical waveguides in SiO_2-Si multi-layer structures, *Appl. Phys. Lett.*, **49**, 13–15, 1986.
27. T. Baba, Y. Kokubun, T. Sakaki, and K. Iga, Loss reduction of an ARROW waveguide in shorter wavelength and its stack configuration, *J. Lightwave Technol.*, **6**, 1440–1445, 1988.
28. P. M. Morse and H. Feshbach, *Methods of Theoretical Physics*, New York: McGraw-Hill, Ch.9, 1953.
29. M. Abramowitz andI. A. Stegun (ed.), *Handbook of Mathematical Functions*, New York: Dover, 446–454, 1970.
30. J. Janta and J. Čtyroký, On the accuracy of WKB analysis of TE and TM modes in planar graded-index waveguides, *Optics Commun.*, **25**, 49–52, 1978.
31. K. S. Chiang, Simplified universal dispersion curves for graded-index planar waveguides based on the WKB method, *J. Lightwave Technol.*, **13**, 158–162, 1995.
32. K. S. Chiang, Review of numerical and approximate methods for the modal analysis of general optical dielectric waveguides, *Opt. Quantum Electron.*, **26**, S113–134, 1994.
33. E. A. J. Marcatili, Dielectric rectangular waveguide and directional coupler for integrated optics, *Bell Syst. Tech. J.*, **48**, 2071–2102, 1969.
34. R. M. Knox and P. P. Toulios, Integrated circuits for the millimeter through optical frequency range, in *Proc. Symp. Submillimeter Waves*, Brooklyn: Polytechnic Press, 497–516, 1970.
35. A. Kumar, K. Thyagarajan, and A. K. Ghatak, Analysis of rectangular-core dielectric waveguides: an accurate perturbation approach, *Opt. Lett.*, **8**, 63–65, 1983.

36. K. S. Chiang, Effective-index analysis of optical waveguides, in *SPIE Proc. Physics and Simulation of Optoelectronic Devices III*, **2399**, 2–12, 1995.
37. K. S. Chiang, Performance of the effective-index method for the analysis of dielectric waveguides, *Opt. Lett.*, **16**, 714–716, 1991.
38. K. S. Chiang, Analysis of the effective-index method for the vector modes of rectangular-core dielectric waveguides' *IEEE Trans. Microwave Theory Tech.*, **44**, 692–700, 1996.
39. K. S. Chiang, Analysis of rectangular dielectric waveguides: effective-index method with built-in perturbation correction, *Electron. Lett.*, **28**, 388–389, 1992.
40. K. S. Chiang, C. H. Kwan, and K. M. Lo, Effective-index method with built-in perturbation correction for the vector modes of rectangular-core optical waveguides, *J. Lightwave Technol.*, **17**, 716–722, 1999.
41. K. S. Chiang, Finite element analysis of weakly guiding fibers with arbitrary refractive-index distribution, *J. Lightwave Technol.*, **LT-4**, 980–990, 1986.
42. L. B. Soldano and E. C. M. Pennings, Optical multi-mode interference devices based on self-imaging: principles and applications, *J. Lightwave Technol.*, **13**, 615–627, 1995.
43. G. B. Hocker and W. K. Burns, Mode dispersion in diffused channel waveguides by the effective index method, *Appl. Opt.*, **16**, 113–118, 1977.
44. P. N. Robson andP. C. Kendall (ed.), *Rib Waveguide Theory by the Spectral Index Method*, New York: Research Studies Press, 1990.
45. K. S. Chiang, Dispersion characteristics of strip dielectric waveguides, *IEEE Trans. Microwave Theory Tech.*, **39**, 349–352, 1991.
46. S. Y. Cheng, K. S. Chiang, and H. P. Chan, Birefringence characteristics of benzocyclobutene rib optical waveguides, *Electron. Lett.*, **40**, 372–373, 2004.
47. J. D. Joannopoulos, R. D. Meade, and J. N. Winn, *Photonic Crystal: Molding the Flow of Light*, Princeton: Princeton University Press, 1995.
48. D. W. Prather, S. Shi, J. Murakowski, G. J. Schneider, A. Sharkawy, C. Chen, and B. Miao, Photonic crystal structures and applications: perspective, overview, and development, *IEEE J. Sel. Top. Quantum. Electron.*, **12**,pp. 1416–1437, 2006.
49. P. Yeh, A. Yariv, and C. S. Hong, Electromagnetic propagation in periodic stratified media. I. General theory, *J. Opt. Soc. Am.*, **67**, 423–438, 1977.
50. Y. Fink, J. N. Winn, S. Fan, C. Chen, J. Michel, J. D. Joannopoulos, and E. L. Thomas, A dielectric omnidirectional Reflector, *Science*, **282**, 1679–1682, 1998.
51. A Taflove and S. C. Hagness, *Computational Electrodynamics: The Finite-Difference Time-Domain Method*, Boston: Artech House, 2005.
52. C. H. Kwan and K. S. Chiang, Effective-index method with built-in perturbation correction for the design of polarization-insensitive optical waveguide directional couplers, *J. Lightwave Technol.*, **20**, 1018–1026, 2002.
53. S. Y. Cheng, K. S. Chiang, and H. P. Chan, Polarization dependence in polymer waveguide directional couplers, *IEEE Photon. Technol. Lett.*, **17**, 1465–1467, 2005.
54. Y. Bai, Q. Liu, K. P. Lor, and K. S. Chiang, Widely tunable long-period waveguide grating couplers, *Optics Express*, **14**, 12644–12654, 2006.
55. S. I. Najafi (ed.), *Introduction of Glass Integrated Optics*, Norwood: Artech House, 1992.
56. S. Janz, A. Bogdanov, P. Cheben, A. Delâge, B. Lamontagne, M.-J. Picard, D.-X. Xu, K. P. Yap, and W. N. Ye, Silicon-based integrated optics: waveguide technology to microphotonics, in *Proc. Mater. Res. Soc. Symp.* **832**, F1.1.1–F1.1.12, 2005.
57. L. Eldada and L. W. Shackelette, Advances in polymer integrated optics, *IEEE J. Sel. Top. Quantum. Electron.*, **6**, 54–68, 2000.
58. K. S. Chiang, K. P. Lor, Q. Liu, and H. P. Chan, UV-written buried waveguides in benzocyclobutene, in *SPIE Proc. Asia-Pacific Optical and Wireless Communications Conference and Exhibition*, **6351**,63511J(1–8), 2006.
59. P. Yang, J. Guo, G. R. Burns, and T. S. Luk, Direct-write embedded waveguides and integrated optics in bulk glass by femosecond laser pulses, *Opt. Eng.*, **44**,051104(1–6), 2005.
60. J. Narasimhan and I. Papautsky, Polymer embossing tools for rapid prototyping of plastic microfluidic devices, *J. Micromech. Microeng.*, **14**, 96–103, 2004.
61. P. K. Tien and R. Ulrich, Theory of prism-coupling and thin film light guides, *J. Opt. Soc. Amer.*, **60**, 1325–1337, 1970.
62. K. S. Chiang, Construction of refractive-index profiles of planar dielectric waveguides from the distribution of effective indexes, *J. Lightwave Technol.*, **LT-3**, 385–391, 1985.
63. K. S. Chiang, Refractive-index profiling of graded-index planar waveguides from effective indexes measured for both mode types and at different wavelengths, *J. Lightwave Technol.*, **14**, 827–832, 1996.
64. K. S. Chiang, C. L. Wong, S. Y. Cheng, and H. P. Chan, Refractive-index profiling of graded-index planar waveguides from effective indexes measured with different external refractive indexes, *J. Lightwave Technol.*, **18**, 1412–1417, 2000.
65. K. Morishita, Index profiling of three-dimensional optical waveguides by the propagation-mode near-field method, *J. Lightwave Technol.*, **LT-4**, 1120–1124, 1986.
66. R. E. Slusher andB. J. Eggleton (ed.), *Nonlinear Photonic Crystals*, Berlin: Springer-Verlag, 2003.
67. A. Yeniay, R. Y. Gao, K. Takayama, R. F. Gao, and A. F. Garito, Ultra-low-loss polymer waveguides, *J. Lightwave Technol.* **22**, 154–158, 2004.
68. L. W. Shacklette, Polymers in the light path: optical polymer technology for communications, *Optics & Photonics News*, **15**, 22–27,Nov. 2004.

KIN SENG CHIANG
Department of Electronic Engineering, City University of Hong Kong, 83 Tat Chee Avenue, Kowloon, Hong Kong